

Superman: Unifying Skeleton and Vision for Human Motion Perception and Generation

Xinshun Wang^{1,*}, Peiming Li^{1,*}, Ziyi Wang^{1,*}, Zhongbin Fang², Zhichao Deng², Songtao Wu³, Jason Li⁴, Mengyuan Liu¹

¹Peking University, ²Sun Yat-sen University, ³Sony R&D Center, ⁴Nanyang Technological University

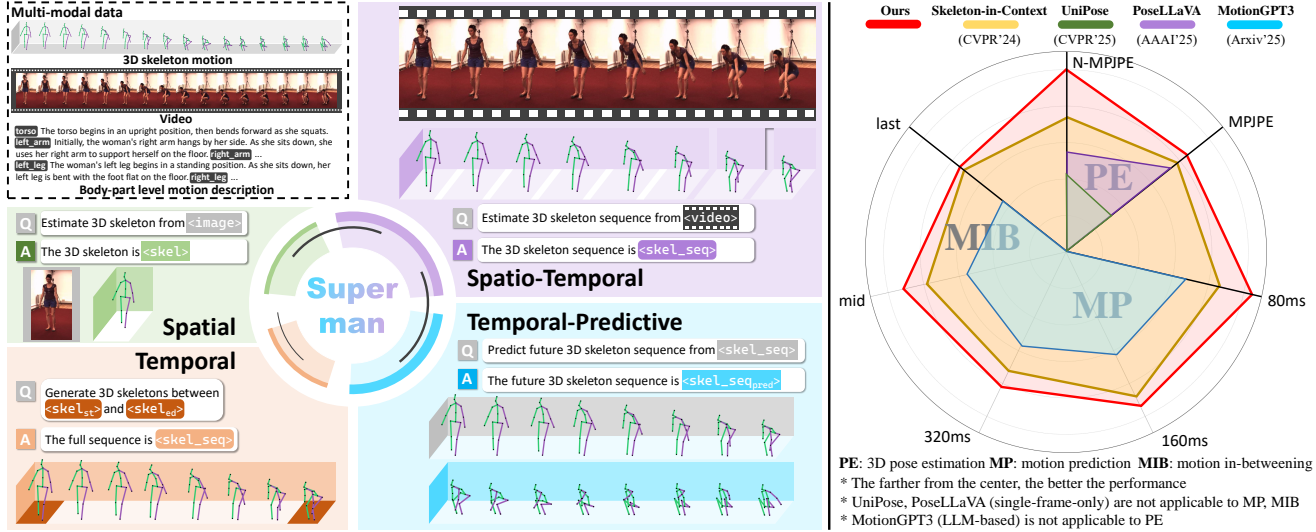


Figure 1. **A Unified Framework for Human Motion Perception and Generation.** Our unified model achieves state-of-the-art performance across three traditionally disparate tasks. Our method consistently outperforms existing methods across all tasks simultaneously: **(1) 3D Pose Estimation**, **(2) Motion Prediction**, and **(3) Motion In-betweening**.

Abstract

Human motion analysis tasks, such as temporal 3D pose estimation, motion prediction, and motion in-betweening, play an essential role in computer vision. However, current paradigms suffer from severe fragmentation. First, the field is split between “perception” models that understand motion from video but only output text, and “generation” models that cannot perceive from raw visual input. Second, generative MLLMs are often limited to single-frame, static poses using dense, parametric SMPL models, failing to handle temporal motion. Third, existing motion vocabularies are built from skeleton data alone, severing the link to the visual domain. To address these challenges, we introduce *Superman*, a unified framework that bridges visual perception with temporal, skeleton-based motion generation. Our solution is twofold. First, to overcome the modality disconnect, we propose a *Vision-Guided Motion Tokenizer*. Leverag-

ing the natural geometric alignment between 3D skeletons and visual data, this module pioneers robust joint learning from both modalities, creating a unified, cross-modal motion vocabulary. Second, grounded in this motion language, a single, unified MLLM architecture is trained to handle all tasks. This module flexibly processes diverse, temporal inputs, unifying 3D skeleton pose estimation from video (perception) with skeleton-based motion prediction and in-betweening (generation). Extensive experiments on standard benchmarks, including Human3.6M, demonstrate that our unified method achieves state-of-the-art or competitive performance across all motion tasks. This showcases a more efficient and scalable path for generative motion analysis using skeletons.

1. Introduction

Human motion analysis is a cornerstone of computer vision and robotics, with critical applications in human-computer interaction, augmented reality, and autonomous systems [1, 18, 34, 35]. Several tasks such as 3D pose estima-

* Equal contribution. Corresponding author is Mengyuan Liu.

Table 1. Comparison with existing traditional and LLM/MLLM-based models for perceiving and/or generating human poses

	Perception	Generation	Tokenizer	Repr.
	vision	motion*	motion*	visual guidance
<i>Traditional Multi-Task Models</i>				
MotionBERT [39]	✗	✓	✗	N/A
SiC [30]	✗	✓	✗	N/A
HiC [19]	✗	✓	✗	N/A
<i>LLM / MLLM-based Models</i>				
MotionLLM [4]	video	✓	✗	SMPL
MotionGPT [14]	✗	✓	✓	SMPL
MotionGPT3 [38]	✗	✓	✓	SMPL
LocLLM [28]	image	✗	✗	✗
PoseLLaVA [9]	image	✗	✗	SMPL
UniPose [16]	image	✗	✗	SMPL
Superman	video&image	✓	✓	✓
				skeleton

* “Motion” refers to a temporal sequence of poses.

tion [18, 34, 35], motion prediction [6, 29, 31], and in-betweening [8, 11, 12, 15, 37] form the core of this field. Traditionally, these tasks have been tackled by highly specialized models, each optimized for a single objective. While this focused approach has yielded significant success, it has led to a fragmented and inflexible ecosystem.

The recent paradigm shift driven by Multi-modal Large Language Models (MLLMs) offers a compelling path toward unification. However, a fundamental disconnect persists, cleaving the field into two distinct camps. On one side, Multi-modal Large Language Models (MLLMs) like MotionLLM [4] and LLaVA-Pose [33] excel at understanding motion. They can reason about poses from raw video and then generate textual descriptions, but lack the capacity to generate new, plausible human poses. On the other hand, specialized generative models like MotionGPT [14] excel at generating motion from text but struggle to process or perceive raw visual inputs. This “read-only” vs. “write-only” dichotomy forces researchers to use disparate architectures for tasks that are inherently interconnected. Moreover, constraints on input modality are also a limitation. Many generative methods operate only on abstract text or single images (*e.g.*, ChatPose [10], PoseLLaVA [9], UniPose [16]), ignoring the rich temporal dynamics of video. Conversely, video-processing models such as SKI Models [22] are typically confined to understanding, not perception, *i.e.*, generating textual results instead of human poses. This fragmentation not only hinders research efficiency but also prevents models from leveraging the synergistic relationship between perception and generation. This leaves a critical gap: the absence of a single, unified model that can fluidly process *multi-modal inputs*, from *full videos* for pose estimation to skeleton sequences for prediction, and generate coherent, structured 3D motion as output.

To unify perception with generation, we conceptualize motion as a universal language. Our core idea is to train a

single MLLM to serve as a unified motion processor. The key to achieving this is a cross-modal motion vocabulary. Existing methods, however, build this vocabulary only from skeletal data, severing the link to the visual domain.

To address this, we introduce **Superman**, a unified, multi-task, and multi-modal generative framework that reformulates these disparate challenges as a conditional sequence generation problem. Our approach has two key advantages: 1) it unifies perception and generation in a single model, promoting knowledge sharing between tasks; 2) it is flexible with multi-modal inputs, processing video, sequential skeletons, and text within the same architecture. Our cornerstone is the Vision-Guided Motion Tokenizer, a VQ-VAE [26] architecture building a universal, discrete pose vocabulary. Unlike prior works limited to skeleton data, our tokenizer introduces a **hybrid codebook** for a richer, cross-modal representation. Each token comprises paired visual and geometric prototypes. This structure guides quantization using both visual appearance from frames and 3D skeleton geometry, creating a powerful representation that intrinsically links visual evidence to motion semantics.

Grounded in this motion language, our MLLM flexibly processes diverse inputs within a single architecture. It can: **(1) Estimate 3D Pose** by translating a video into a sequence of pose tokens. **(2) Predict Motion** by auto-regressively completing a pose sequence. **(3) Perform In-betweening** by generating intermediate tokens between keyframes. As shown in Fig. 1, our unified design is validated by extensive experiments on standard benchmarks including Human3.6M [13] and 3DPW [27]. Superman achieves state-of-the-art performance across all tasks, even when compared with traditional multitask models specializing in perception tasks. For instance, for 3D pose estimation on Human3.6M [13], Superman achieves an 11.97% improvement compared with the state-of-the-art multi-task perception method [19], and a 10.91% improvement compared with the state-of-the-art LLM/MLLM-based method [9]. Additionally, Superman delivers strong generalization performance. Trained exclusively on Human3.6M, Superman generalizes well to unseen data, namely 3DPW [27], and outperforms existing methods. Our contributions are three-fold:

- We propose a unified generative framework that leverages a single MLLM for multi-task, multi-modal human motion analysis, bridging the gap between motion perception and generation.
- We introduce a novel Vision-Guided Motion Tokenizer that creates a robust, cross-modal pose vocabulary. By designing a hybrid codebook where each token is a bimodal entity comprising paired visual and geometric prototypes, we ensure that the quantization process is simultaneously guided by both appearance features from video and the geometric structure of 3D skeletons.

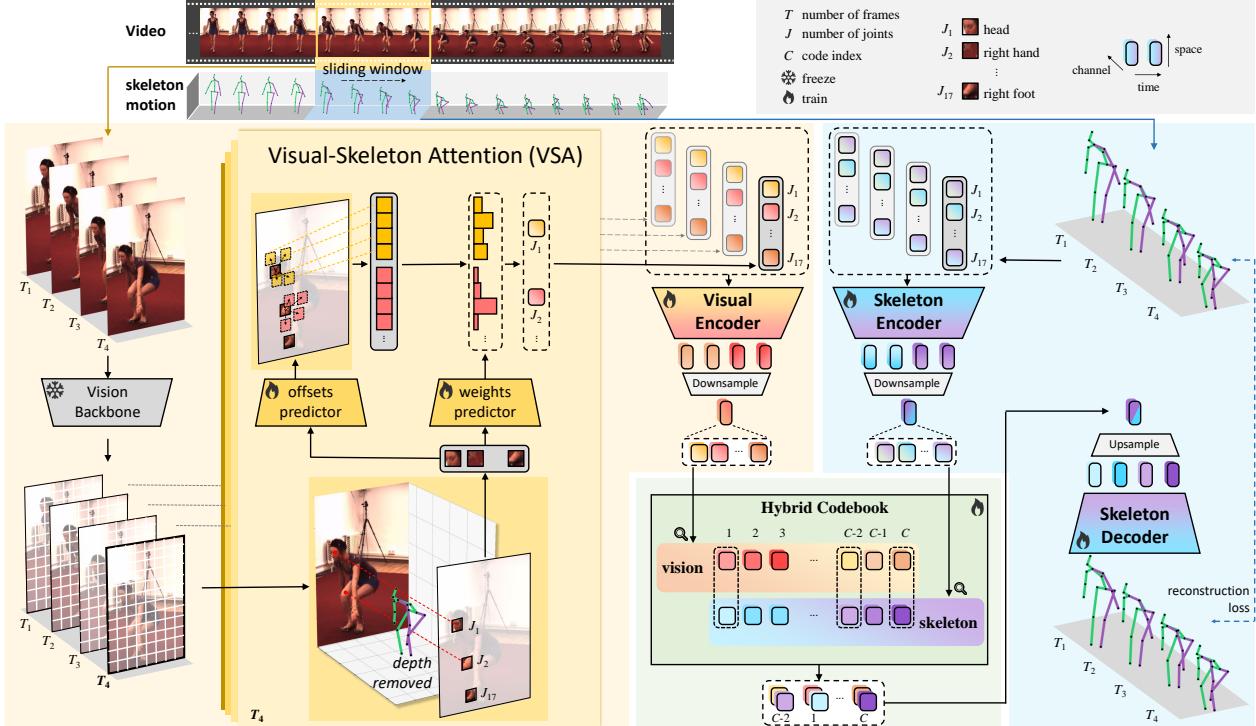


Figure 2. **Architecture of our Vision-Guided Motion Tokenizer (VGMT).** VGMT creates a discrete motion vocabulary by jointly fusing information from two modalities. A Skeleton Encoder (E_s) captures geometry while a Visual-Skeleton Attention (VSA) module and a subsequent Visual Encoder (E_v) ground the pose in visual features. The fused representation is quantized against a learnable hybrid codebook, and a decoder reconstructs the 3D poses.

- We demonstrate that our unified method achieves state-of-the-art across diverse tasks, validating the efficacy and scalability of our approach.

2. Related Work

3D Human Pose Estimation. 3D human pose estimation has evolved from classical methods to deep learning approaches using CNNs [25] and Transformers [36] to model human body structure. Modern methods typically follow a two-stage pipeline of lifting 2D keypoints to 3D [20] or perform end-to-end regression from images [24], while capturing spatio-temporal relationships to ensure temporal coherence [21]. However, a common thread among these methods [20, 21, 24, 36] is their specialization on the single task of pose estimation. In contrast, our work integrates pose estimation into a unified generative framework, allowing the model to perform both perception and generation tasks, rather than being confined to a single objective.

Human Motion as a Language. A groundbreaking shift in motion analysis involves representing continuous human motion as a sequence of discrete tokens, a paradigm pioneered by early works in gesture synthesis [14]. A common technique for this is using a Vector Quantized Variational Autoencoder (VQ-VAE) to learn a “codebook” of atomic poses. As summarized in Tab. 1, recent models have

framed tasks like motion generation and prediction as language modeling problems [14, 35]. However, their scope is often limited to generating from non-visual modalities, failing to ground the motion language in raw visual input. Our work builds directly upon this paradigm but makes a crucial extension by integrating vision into the tokenization process, creating a visually grounded motion language.

Multi-modal Large Language Models for Pose Perception and Generation. The remarkable success of Multi-modal Large Language Models (MLLMs), which integrate powerful vision encoders with LLMs for complex visual reasoning [7, 17, 32], has inspired their application to human-centric tasks. In the context of human motion, models such as MotionLLM [4] and LLaVA-Pose [33] have demonstrated the ability to comprehend and answer questions about human actions and poses depicted in images and videos. They effectively connect the visual and semantic aspects of human motion. However, a significant limitation of these models is their primary focus on perception. They can interpret and describe poses, but they are not architecturally designed to generate new, structured motion sequences. Recent works, such as ChatPose [10] and UniPose [16], have begun to bridge this gap by enabling pose generation conditioned on both visual and textual inputs. These models, however, typically operate on static, single-frame images. Our work distinguishes itself by being a fully

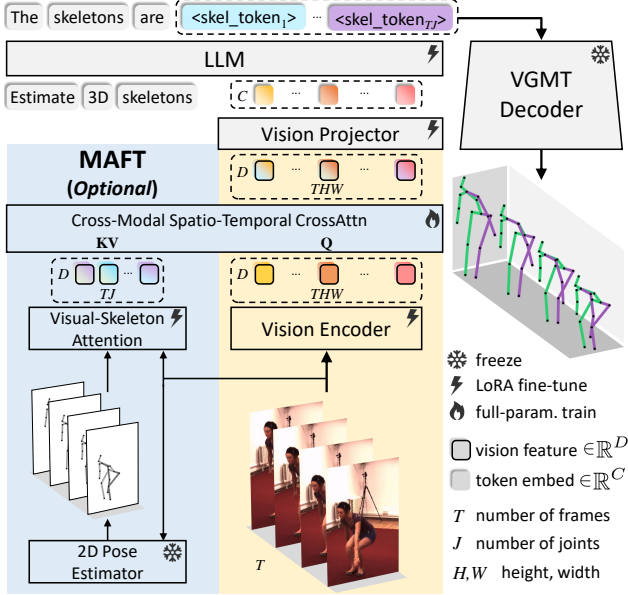


Figure 3. **Network architecture and training paradigm.** Superman fine-tune a single LLM to integrate information from text, video, and 3D skeleton modalities. Optionally, a **Motion-Aware Fine-Tuning (MAFT)** module can be integrated. With <0.2% extra parameters, MAFT enhances motion perception by enabling cross-video-motion fusion, leading to substantial improvement on tasks with visual input, as validated by the experiment results.

versatile framework that not only perceives motion from videos but is also a powerful generative model capable of multiple synthesis tasks, thereby unifying the reading and writing of motion within a single, coherent architecture.

3. Method

Our method unifies multi-task human motion analysis within a conditional sequence generation framework. It involves two key stages: (1) a novel **Vision-Guided Motion Tokenizer** (Section 3.1) that converts continuous, high-dimensional motion into a discrete sequence of semantic tokens, and (2) a **Multi-modal Large Language Model (MLLM)** (Section 3.2) that autoregressively models these token sequences to perform our diverse set of tasks. The overall network architecture is depicted in Fig. 3.

3.1. Vision-Guided Motion Tokenizer

The cornerstone of our approach is a discrete vocabulary for continuous human motion. Unlike prior tokenizers that rely on skeletons alone [14], we design a Vision-Guided Motion Tokenizer, built upon a VQ-VAE, which is explicitly trained to fuse *visual appearance* and *3D skeletal geometry*. This ensures each token is grounded in both modalities. The architecture is illustrated in Fig. 2.

Dual-Stream Encoding. Given a video clip $\mathcal{V} \in \mathbb{R}^{F \times H \times W \times 3}$ and its corresponding 3D pose sequence $\mathbf{X} \in$

$\mathbb{R}^{F \times N \times 3}$, our tokenizer employs two parallel streams.

1) *Visual Encoding Stream*: This stream extracts pose-centric visual features. We first use a vision backbone (e.g., HRNet [23]) to obtain feature maps \mathcal{F}_f for each frame. For each joint j at frame f , its projected 2D location $\mathbf{p}_{j,f}$ serves as a reference point to sample an initial query feature $\mathbf{q}_{j,f}$ from \mathcal{F}_f . To enhance feature representation and robustness to occlusions, we introduce a Visual-Skeleton Attention (VSA) module. The VSA adaptively aggregates features by predicting sampling offsets and aggregation weights from the query. The visual feature for the joint is computed as:

$$\mathbf{v}_{j,f} = \text{VSA}(\mathbf{q}_{j,f}, \mathcal{F}_f, \mathbf{p}_{j,f}), \quad (1)$$

yielding a sequence of contextually-aware visual features $\mathbf{V} \in \mathbb{R}^{F \times N \times D}$.

2) *Skeletal Encoding Stream*: This stream captures the motion’s intrinsic geometry. The input pose sequence \mathbf{X} is passed through a series of lightweight 2D convolutions operating on the joint-temporal grid. This effectively models spatio-temporal kinematics and maps the coordinates into a latent space, producing skeletal features $\mathbf{S} \in \mathbb{R}^{F \times N \times D}$.

Hybrid Codebook Quantization. To ensure each token represents a short *motion pattern* rather than a static pose, we first temporally downsample the feature sequences \mathbf{V} and \mathbf{S} , yielding window-level representations \mathbf{z}_w^v and \mathbf{z}_w^s for each time window w . We then introduce a hybrid codebook that pairs visual and geometric prototypes: $\mathcal{C} = \{(\mathbf{c}_k^v, \mathbf{c}_k^s)\}_{k=1}^K$, where $\mathbf{c}_k^v, \mathbf{c}_k^s \in \mathbb{R}^D$. For each window w , k_w is the token index that minimizes the joint distance:

$$k_w = \arg \min_k (\|\mathbf{z}_w^v - \mathbf{c}_k^v\|_2^2 + \|\mathbf{z}_w^s - \mathbf{c}_k^s\|_2^2). \quad (2)$$

This hybrid selection, based on minimizing the joint Euclidean distance, grounds the discretization process in both vision and geometry. The selected code vectors for the window are then $\hat{\mathbf{c}}_w^v = \mathbf{c}_{k_w}^v$ and $\hat{\mathbf{c}}_w^s = \mathbf{c}_{k_w}^s$.

Reconstruction and Training. The skeletal code $\hat{\mathbf{c}}_w^s$ is upsampled and passed to a decoder to reconstruct the 3D poses $\hat{\mathbf{X}}_w$. The tokenizer is trained end-to-end with a VQ objective that combines reconstruction with modality-wise commitment losses:

$$\mathcal{L}_{\text{VQ}} = \|\mathbf{X}_w - \hat{\mathbf{X}}_w\|_2^2 + \beta_s \|\text{sg}[\mathbf{z}_w^s] - \hat{\mathbf{c}}_w^s\|_2^2 + \beta_v \|\text{sg}[\mathbf{z}_w^v] - \hat{\mathbf{c}}_w^v\|_2^2, \quad (3)$$

where $\text{sg}[\cdot]$ is the stop-gradient operator, and we set the commitment weights $\beta_s = 0.5$ and $\beta_v = 0.5$. This process effectively converts a continuous motion clip of F frames into a discrete sequence of T integer tokens $\mathbf{K}_{1:T}$. After training, the tokenizer provides a robust, visually-grounded motion vocabulary.

3.2. Unified Multi-Task Modeling with LLM

Our discrete motion tokenizer enables us to frame diverse motion tasks as a unified conditional sequence generation problem. We employ a decoder-only Multi-modal Large

Table 2. **Comparison of our model with traditional multi-task models and LLM / MLLM-based models** on three human motion tasks: pose estimation (PE), motion prediction (MP), and motion in-betweening (MIB) on Human3.6M [13]. All tasks are evaluated using Mean Per Joint Position Error (MPJPE) in millimeters, averaged over all test data, where lower is better. “ T ” means how many frames the model inputs and outputs. (“ $T=1$ ” means the video has to be processed image-by-image.) “N/A” means the model is not applicable to the task. For example, single-frame-only models [9, 16, 28] cannot do MP or MIB; LLM-based models [14, 38] cannot do PE.

Models	Venue	T	PE ‡		MP †				MIB †			
			N-MPJPE	MPJPE	Avg	80ms	160ms	320ms	Avg	mid	last	
<i>Traditional Multi-Task Models</i>												
MotionBERT [39]	ICCV’23	16	47.07	56.70	29.94	18.67	26.82	50.33	42.37	44.86	53.16	
Skeleton-in-Context [30]	CVPR’24	16	45.26	55.57	33.42	21.09	30.48	54.62	31.27	36.66	36.84	
Human-in-Context [19]	Arxiv’25	16	44.77	53.86	26.66	14.36	23.58	47.34	31.13	37.01	35.49	
Superman (w/ MAFT)	Ours’26	16	39.41	51.61	26.13†	13.70	23.30	44.90	30.61†	35.99	35.13	
<i>LLM / MLLM-based Models</i>												
LocLLM [28]	CVPR’24	1	49.32	62.19	N/A				N/A			
UniPose [16]	CVPR’25	1	65.24	106.96	N/A				N/A			
PoseLLaVA [9]	AAAI’25	1	50.40	62.43	N/A				N/A			
MotionGPT [14]	NeurIPS’23	16	N/A		48.81	42.99	49.27	55.31	52.96	56.07	66.45	
MotionGPT3 [38]	Arxiv’25	16	N/A		42.30	37.25	42.70	47.94	47.66	50.47	59.81	
Superman	Ours’26	16	44.90	61.39	26.13†	13.70	23.30	44.90	30.61†	35.99	35.13	

\ddagger Traditional models adopt “RGB \rightarrow 2D \rightarrow 3D” paradigm, leveraging a fixed 2D pose estimator; LLM/MLLM-based models adopt “RGB \rightarrow 3D” paradigm.

\dagger For MP and MIB, existing methods take only 3D poses as input (no vision). For fair comparison, our MAFT module (which enhances vision) is not active, hence the identical results for Superman and Superman (w/ MAFT) on these tasks.

Language Model (MLLM), Qwen2.5-VL-7B [2], as our central sequence processor, which learns to predict motion tokens autoregressively.

Connecting Tokenizer to Qwen-VL. Besides the standard tokenizer-MLLM integration paradigm [14, 16], we additionally design an optional light-weight module to inject skeletal geometry into the MLLM’s visual stream, Motion-Aware Fine-tuning (MAFT). First, we enhance the ViT features using a Visual-Skeleton Attention (VSA) block. The ViT backbone extracts patch features \mathbf{Z}_{grid} . Concurrently, 2D joint projections serve as reference points for a multi-scale deformable sampler [40] to aggregate pose-centric features \mathbf{Z}_{pose} . We then fuse this information using VSA, implemented as a cross-attention layer followed by an FFN, where grid tokens are queries and pose tokens are keys/values. The visual tokens $\hat{\mathbf{Z}}_{\text{grid}}$ are computed as:

$$\hat{\mathbf{Z}}_{\text{grid}} = \text{VSA}(\mathbf{Z}_{\text{grid}}, \mathbf{Z}_{\text{pose}}). \quad (4)$$

These enhanced visual tokens, along with any textual prompts, are fed into the LLM decoder, which generates the final sequence of motion tokens.

Our framework handles multiple tasks by varying the conditioning inputs:

3D Pose Estimation from Video: Given a video clip $\mathbf{I}_{1:F}$, the MLLM is conditioned on its enhanced visual

features $\hat{\mathbf{Z}}_{\text{grid}}$ to generate the corresponding motion token sequence $\mathbf{K}_{1:T}$. The objective is to maximize the log-likelihood of the ground-truth sequence:

$$\mathcal{L}_{\text{est}} = \sum_{t=1}^T \log P(k_t | \mathbf{K}_{<t}, \hat{\mathbf{Z}}_{\text{grid}}). \quad (5)$$

The tokens are then decoded to obtain the final 3D poses.

Motion Prediction: Given a historical pose sequence, tokenized as $\mathbf{K}_{1:T'}$, the task is to predict the future. The LLM autoregressively generates subsequent tokens $\mathbf{K}_{T'+1:T}$ conditioned on the past:

$$\mathcal{L}_{\text{pred}} = \sum_{t=T'+1}^T \log P(k_t | \mathbf{K}_{<t}). \quad (6)$$

Motion In-betweening: Given start and end tokens (k_1, k_T), we use a prompt like “[START] k_1 [MIDDLE] k_T [END]”, training the LLM to fill in the missing sequence corresponding to the [MIDDLE] segment.

Our framework’s strength is a single LLM trained jointly on a mixture of task-specific formats. This multi-task strategy fosters a rich, unified representation, allowing it to act as a versatile motion processor.

Table 3. Action-specific N-MPJPEs for pose estimation on Human3.6M [13].

Models	Venue	T	Actions							
			Sit	SitDown	Smoke	Photo	Wait	Walk	WalkDog	WalkTwo
<i>Traditional Multi-Task Models</i>										
MotionBERT [39]	ICCV'23	16	62.22	69.81	49.21	49.66	39.49	40.80	44.94	40.95
Skeleton-in-Context [30]	CVPR'24	16	59.34	65.89	48.70	48.11	37.28	38.52	42.12	38.97
Human-in-Context [19]	Arxiv'25	16	59.95	65.21	47.81	47.02	36.37	38.17	41.76	37.31
Superman (w/ MAFT)	Ours'26	16	47.12	48.97	41.31	34.37	41.21	36.12	39.23	43.23
<i>LLM / MLLM-based Models</i>										
LocLLM [28]	CVPR'24	1	64.48	68.76	50.96	55.16	42.55	39.11	49.96	43.10
UniPose [16]	CVPR'25	1	72.30	84.24	69.20	62.65	60.02	66.97	65.71	70.69
PoseLLaVA [9]	AAAI'25	1	64.64	71.36	52.67	54.21	44.67	46.90	48.90	44.90
Superman	Ours'26	16	62.68	71.93	49.09	43.54	35.21	30.89	45.91	39.60
Models	Venue	T	Actions							
			Direct	Discuss	Eat	Greet	Phone	Pose	Purchase	
<i>Traditional Multi-Task Models</i>										
MotionBERT [39]	ICCV'23	16	39.85	46.10	41.77	43.35	46.57	42.04	43.72	
Skeleton-in-Context [30]	CVPR'24	16	38.03	44.23	41.15	41.97	45.26	40.09	41.95	
Human-in-Context [19]	Arxiv'25	16	37.51	44.30	40.30	41.33	44.74	39.68	42.02	
Superman (w/MAFT)	Ours'26	16	42.72	36.50	33.65	35.06	40.77	34.21	36.16	
<i>LLM / MLLM-based Models</i>										
LocLLM [28]	CVPR'24	1	42.12	49.09	41.70	44.22	51.81	45.04	43.70	
UniPose [16]	CVPR'25	1	52.57	61.62	59.55	60.33	71.57	54.79	63.35	
PoseLLaVA [9]	AAAI'25	1	43.00	47.80	45.64	47.58	49.21	44.49	47.16	
Superman	Ours'26	16	34.74	43.09	45.01	36.03	48.98	34.28	44.90	

Table 4. Comparison of results on generalization to unseen data. Motion prediction (MP) and motion in-betweening (MIB) on 3DPW [27] are reported. All models are only trained on Human3.6M, with 3DPW completely excluded from training.

Models	MP			MIB	
	Avg	80ms	320ms	Avg	mid
<i>Traditional Multi-Task Models</i>					
MotionBERT [39]	164.96	137.89	200.14	123.05	148.51
Skeleton-in-Context [30]	140.71	110.77	183.74	103.97	127.68
Human-in-Context [19]	141.90	112.53	183.62	108.54	131.99
<i>LLM / MLLM-based Models</i>					
MotionGPT [14]	292.87	257.92	331.88	234.39	257.55
MotionGPT3 [38]	228.17	190.83	259.49	180.10	204.71
Superman (Ours)	62.05	34.75	97.37	60.68	63.35

Training. Our framework is trained in two stages. First, the Vision-Guided Motion Tokenizer is trained independently, with its weights frozen. Subsequently, the MLLM is trained on a mixture of all tasks using a single, unified objective: the standard autoregressive cross-entropy loss, summed across all task-specific samples in a batch. This joint strategy facilitates knowledge transfer between perception and generation.

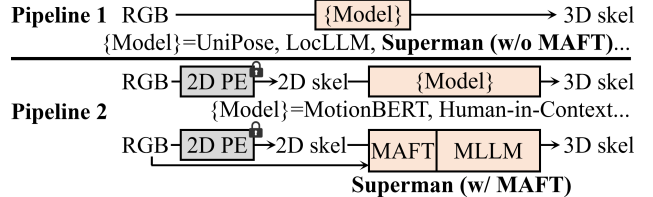


Figure 4. Two standard pipelines for 3D pose estimation. “2D PE” means 2D pose estimator. “skel” is short for skeleton.

4. Experiment

Implementation Details. 1) *Vision-Guided Motion Tokenizer (VGMT).* The VGMT adopts a dual-stream architecture. The vision backbone consists of a standard HRNet-w48 [23] without the heatmap head (frozen). The Skeleton Encoder comprises 2 layers of 2D convolutions with residual connections, followed by 1 convolutional downsampling layers, reducing the number of frames by half. The Visual Encoder has an identical structure to the Skeleton Encoder without the first 2D convolutional layer, as the HRNet already projects the visual features to the latent space. Both skeletal and visual features have 1024 dimensions, half of the dimensions of the codebook. The Hybrid Codebook contains $K = 8192$ codes, with a dimension of $D = 2048$. The Decoder mirrors the encoder structure with upsampling layers to reconstruct the 16-frame sequence.

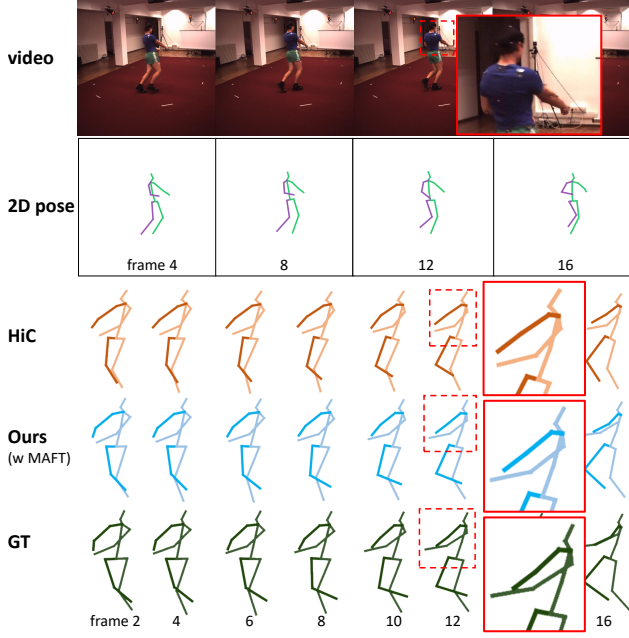


Figure 5. Qualitative results for pose estimation on Human3.6M. Our method with MAFT is compared with HiC [19], the current SoTA. Both methods use video and 2D poses as inputs and leverage a fixed 2D pose estimator.

2) *Unified MLLM*. We use Qwen2.5-VL-7B as the base model. We apply LoRA (Low-Rank Adaptation) to the linear layers of the self-attention modules ($q\text{-}proj$, $v\text{-}proj$) with a rank $r = 8$. The MAFT module consists of a single cross-attention layer with 8 heads and a hidden dimension of 1280 (the same as the vision embeddings in Qwen2.5-VL-7B), followed by a standard FFN. The total parameter size of Qwen2.5-VL-7B is 9,605M. Without MAFT, the trainable parameter size is 1,210M, 12.67% of the total parameters. With MAFT, the trainable parameter size is 1,235M, 12.87% of the total parameters. The MAFT introduces $< 0.2\%$ extra parameters. The model is trained on 2 NVIDIA H20 GPUs.

Datasets and Metrics. For evaluation, we utilize two large-scale 3D human motion datasets: Human3.6M [13] and 3DPW [27]. The models are trained on Human3.6M only, and tested on both datasets. The training set and the test set are in line with their respective splitting standards. Tasks are evaluated using Mean Per Joint Position Error (MPJPE) as the main metric, in line with standard protocols.

For the task of pose estimation, specifically, there are two mainstream paradigms, as shown in Fig. 4, which traditional and LLM/MLLM-based methods follow, respectively. For fair comparison, we strictly follow both paradigms in the comparison of our method with the respective methods.

Data Preprocessing. To unify formats, we first convert 3DPW’s SMPL vertices to the Human3.6M skeleton format

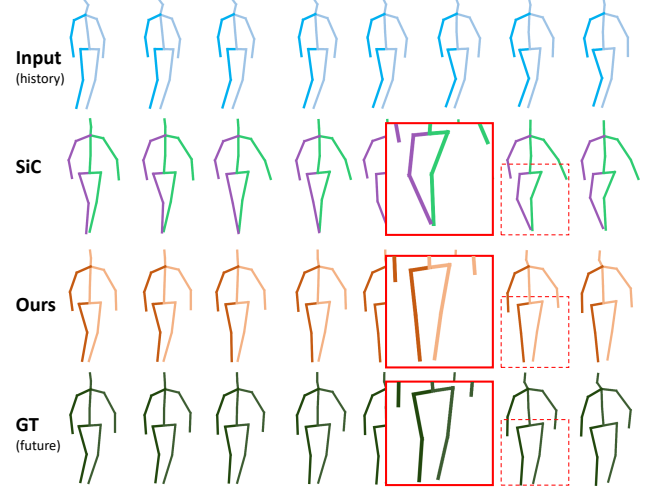


Figure 6. Qualitative results for generalizing to motion prediction on 3DPW (unseen dataset). Our method is compared with SiC [19], the current SoTA on the task.

using a pre-trained matrix [3]. Then, both datasets follow the same processing pipeline. Specifically, for the X and Y spatial dimensions, we transform the 3D camera coordinates (in millimeters) into 2D image coordinates (in pixels), following [39]. For the depth (Z) dimension, we normalize the skeleton by setting the depth of the root joint (pelvis) to 0. The depths of all other joints are then converted to be relative to this root. Crucially, we do not translate the root joint to the coordinate origin (0, 0, 0) during either the training or testing phases. This approach retains the global positional information in the image coordinate space.

4.1. Main Results

Our unified model, Superman, was evaluated on three human motion tasks: 3D Pose Estimation (PE), Motion Prediction (MP), and Motion In-Betweening (MIB). As shown in Tabs. 2, 3, and 4, our model demonstrates state-of-the-art (SOTA) performance on both the standard benchmark (Human3.6M [13]) and generalization tests (3DPW [27]).

Performance on Human3.6M. In the comprehensive evaluation (Tab. 2), our model surpassed all baselines under both paradigms. On the pose estimation task, compared to traditional multi-task models (which use a “RGB→2D→3D” paradigm), Superman achieved 51.61 MPJPE and 39.41 N-MPJPE, the lowest of all models. Compared to LLM/MLLM-based models (which use a “RGB→3D” paradigm), Superman also secured the best performance with 61.39 MPJPE and 44.90 N-MPJPE. In the action-specific N-MPJPE breakdown (Tab. 3), Superman achieved the lowest error in most of the 15 action categories. On the motion prediction and in-betweening tasks, our model also achieves state-of-the-art performance.

Generalization on 3DPW. To evaluate the model’s abil-

Table 5. Computation efficiency.

Module	GFLOPs	params (M)	latency (ms)
<i>Vision-Guided Motion Tokenizer (VGMT)</i>			
vision backbone	31.375	28.53	43.7
vision encoder	2.468	17.12	2.7
VSA	0.001	0.11	0.1
<i>MLLM</i>			
MAFT	5.01	25.45	0.3
Qwen2.5-VL-7B	~129920.00	9605.00	3300.0

* Vision backbone remains frozen during training.

ity to generalize to unseen data, we conduct a zero-shot test on the 3DPW dataset; all models are trained only on Human3.6M and tested on 3DPW. As shown in Tab. 4, Superman demonstrates exceptional generalization on both motion tasks, outperforming all baseline models by a significant margin. Fig. 6 provides qualitative validation for this, showing our model generating more accurate future poses than the current SoTA baseline [30]. On motion inbetweening (MIB), our model achieved an average error of 60.68, again far surpassing the best traditional model (103.97 for Skeleton-in-Context) and other LLM/MLLM models (180.10 or higher).

These results confirm that our model not only excels on the benchmark dataset but also possesses superior robustness and generalization capabilities when handling unseen “in-the-wild” data.

Computational Efficiency. Tab. 5 provides a comprehensive computational profile of the proposed framework, breaking down the efficiency metrics for both the Vision-Guided Motion Tokenizer (VGMT) and the MLLM components. Specifically, it details GFLOPs, parameter counts, and latency for the vision backbone, vision encoder, and VSA. While the large-scale Qwen2.5-VL-7B dominates overall resource consumption, accounting for 99.7% of the total GFLOPs and 98.6% of the total latency, our newly introduced components, such as MAFT and VSA, exhibit remarkably low overhead. Collectively, these proposed modules account for less than 0.03% of the total computation cost, demonstrating the exceptional efficiency and practical scalability of our architecture.

4.2. Visualization

Analysis of the VQ-VAE Codebook. To evaluate the efficiency of our codebook utilization, we conducted a quantitative analysis. As shown in Fig. 7 (a), the codes are categorized into four usage frequency levels: Frequent (usage rate $>1\%$), Active (0.01%–1%), Underused (0–0.01%), and Unused (never used). On the Human3.6M dataset, up to 65.4% of the codes remain Active, indicating efficient utilization of the encoding space. This high efficiency is maintained even

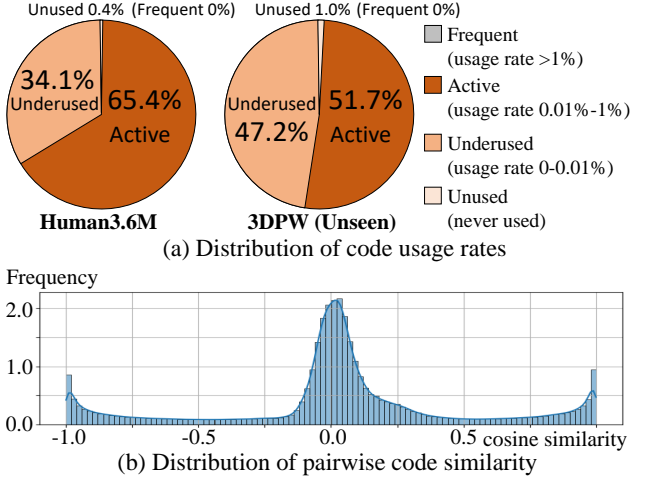


Figure 7. Quantitative analysis of the VQ-VAE codebook. (a) Up to 65.4% of the codes remain Active during inference, indicating efficient usage of the encoding space. (b) The cosine similarity of most code pairs is close to 0, confirming the ability to learn a discrete latent space with highly decorrelated representations.

on the unseen 3DPW dataset, which shows 51.7% Active codes and only 1.0% Unused codes. Furthermore, we analyzed the codebook’s latent space by computing pairwise cosine similarities. The distribution in Fig. 7 (b) shows that the similarity of most code pairs is close to 0, confirming the model’s ability to learn a discrete latent space with highly decorrelated representations.

Qualitative Results for 3D Pose Estimation. Figure 5 presents qualitative visualizations for 3D pose estimation on Human3.6M. The figure provides an intuitive comparison of our model (“Ours” shown in blue) against the baseline method HiC [19] (“HiC” shown in orange) and the Ground Truth (“GT” shown in dark green). Visually, the 3D skeleton sequence generated by our method shows a high degree of fidelity to the Ground Truth in both shape and motion, while the baseline method exhibits noticeable visual discrepancies.

4.3. Ablation Study and Analysis

We conduct comprehensive ablation studies to validate the effectiveness of our framework’s key design choices.

Benefits of Visual Grounding. In addition to the benefits of visual grounding in the pose estimation (PE) task (as evidenced by MAFT), here we also explore the benefits of visual grounding in motion prediction (MP) and inbetweening (MIB) tasks, which are evaluated in the main results (Tab. 2) using only skeleton inputs to ensure a fair comparison with existing methods. Tab. 6 quantifies the substantial performance gains achieved by incorporating visual grounding into MP and MIB tasks. While skeleton-only inputs provide a strong baseline, the integration of raw

Table 6. Impact of visual grounding by adding visual input in motion prediction and in-betweening.

Task	MP ↓			MiB ↓		
	skel	video	skel&video	skel	video	skel&video
Superman	26.13	29.74	23.30	30.61	33.14	25.63

Table 7. Impact of VSA and MAFT on pose estimation.

Architecture	VSA	MAFT	PE (N-MPJPE) ↓
Baseline	✗	✗	48.8
VSA only	✓	✗	44.9
MAFT only	✗	✓	42.2
Superman	✓	✓	39.4

video features (skel&video) significantly reduces prediction errors. These results demonstrate that visual grounding offers critical contextual and spatial cues that are absent in abstract skeleton data. By grounding the generation process in visual evidence, our model captures richer motion semantics, leading to higher fidelity and more physically plausible motion sequences across diverse generative scenarios.

Analysis of Model and Codebook Scaling. To validate the scalability of our framework, we investigate the impact of both the MLLM’s parameter size and the codebook’s capacity. As illustrated in Fig. 8, we evaluate performance (MPJPE) by scaling the model from 3B, 7B to 8B parameters, while simultaneously increasing the codebook scale (in terms of both size and dimension). The 8B version is built upon Qwen3-VL-8B. The results show a clear and consistent trend: (1) Increasing the model size from 3B, 7B to 8B significantly reduces the error for both Pose Estimation (PE) and Motion Prediction (MP). (2) Within a given model size, increasing the codebook capacity (e.g., from 4096×1024 to 4096×2048 for the 3B model) also consistently lowers the MPJPE. This analysis confirms that our unified framework benefits from larger model and codebook parameters, demonstrating strong scalability and potential for future improvements.

Impact of VSA and MAFT. Tab. 7 presents an ablation study evaluating the individual and collective contributions of the Visual-Skeleton Attention (VSA) and Motion-Aware Fine-Tuning (MAFT) modules on 3D pose estimation performance. Starting from a baseline without either, the integration of VSA alone reduces the error, while employing MAFT independently yields a stronger improvement. The “Superman” configuration, which combines both components, achieves the superior performance of 39.4 N-MPJPE. These results confirm that while both modules independently enhance visual-geometric grounding, their synergistic integration provides the most robust motion perception, justifying their inclusion in our default architecture.

Effectiveness of the Vision-Guided Tokenizer. We validate our tokenizer design in Table 8. Results show

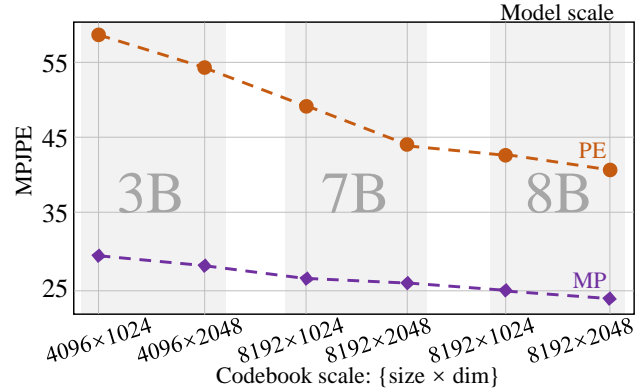


Figure 8. Scaling analysis of model and codebook parameters. Scaling up the model (3B → 7B → 8B) and the codebook consistently reduces (N)-MPJPE for both pose estimation (PE) and motion prediction (MP) tasks, demonstrating the method’s ability to leverage larger capacity for improved accuracy.

Table 8. Ablation on tokenizer components and fusion weights.

Tokenizer Config.	Recon. Err.	PE (N-MPJPE)	MP (N-MPJPE)
		w/o MAFT	w/ MAFT
Visual-Only	22.5	51.3	47.9
Skeleton-Only	7.7	47.8	43.1
Fused: $\beta_s, \beta_v = 0.3, 0.7$	6.8	45.8	40.7
Fused: $\beta_s, \beta_v = 0.7, 0.3$	5.3	45.1	40.3
Fused: $\beta_s, \beta_v = 0.5, 0.5$	4.7	44.9	39.4

that jointly learning from vision and geometry is essential. The Visual-Only model fails (22.5 mm error), and while the Skeleton-Only baseline [14] is reasonable (7.7 mm), it is significantly outperformed by all fused configurations. Among these, our chosen balanced weighting ($\beta_s = 0.5, \beta_v = 0.5$) achieves the lowest reconstruction error (4.7 mm), proving superior to other weightings (5.3–6.8 mm) and validating our approach.

Effectiveness of Unified Multi-Task Training. Effectiveness of Unified Multi-Task Training. Our second key design is the use of a single MLLM for joint multi-task training (as described in Sec. 3.2). To validate this, we compare our Unified model against Specialized models, which use the same architecture but are trained exclusively on a single task. As shown in Tab. 9, our Unified model consistently outperforms its Specialized counterparts across all three tasks. The unified model achieves a PE of 44.9 (vs. 46.5), an MP of 26.1 (vs. 27.3), and an MiB of 30.6 (vs. 33.1). This strongly indicates positive knowledge transfer between tasks, as learning them jointly improves performance in all areas. This confirms our unified framework is not only efficient but also more effective by learning a richer, joint representation.

Table 9. Ablation on the unified multi-task training strategy. We compare our single unified model against specialized models.

Training Strategy	PE	MP	MIB
Specialized (Est. Only)	46.5	N/A	N/A
Specialized (Pred. Only)	N/A	27.3	N/A
Specialized (MiB. Only)	N/A	N/A	33.1
Unified	44.9	26.1	30.6

5. Conclusion

We propose a unified generative framework that bridges the gap between motion perception and generation. The core of our approach is a novel Vision-Guided Motion Tokenizer, which, unlike prior work, learns a robust cross-modal vocabulary by jointly fusing visual features and geometric data. Grounded in this motion language, our single MLLM architecture achieves state-of-the-art or competitive performance across diverse tasks, including 3D pose estimation, motion prediction, and motion in-betweening. This work demonstrates that a unified, visually grounded generative model is an efficient, scalable paradigm for holistic human motion analysis.

References

- [1] Mykhaylo Andriluka, Umar Iqbal, Eldar Insafutdinov, Leonid Pishchulin, Anton Milan, Juergen Gall, and Bernt Schiele. Posetrack: a benchmark for human pose estimation and tracking. In *CVPR*, 2018. [1](#)
- [2] Shuai Bai, Keqin Chen, Xuejing Liu, Jialin Wang, Wenbin Ge, Sibo Song, Kai Dang, Peng Wang, Shijie Wang, Jun Tang, et al. Qwen2. 5-vl technical report. *arXiv preprint arXiv:2502.13923*, 2025. [5](#)
- [3] Federica Bogo, Angjoo Kanazawa, Christoph Lassner, Peter Gehler, Javier Romero, and Michael J Black. Keep it smpl: automatic estimation of 3d human pose and shape from a single image. In *ECCV*, 2016. [7](#)
- [4] Ling-Hao Chen, Shunlin Lu, Ailing Zeng, Hao Zhang, Benyou Wang, Ruimao Zhang, and Lei Zhang. Motionllm: Understanding human behaviors from human motions and videos. *arXiv preprint arXiv:2405.20340*, 2024. [2, 3](#)
- [5] Yilun Chen, Zhicheng Wang, Yuxiang Peng, Zhiqiang Zhang, Gang Yu, and Jian Sun. Cascaded pyramid network for multi-person pose estimation. In *Proceedings of the IEEE conference on computer vision and pattern recognition*, pages 7103–7112, 2018. [2, 3](#)
- [6] Qiongjie Cui and Huaijiang Sun. Towards accurate 3d human motion prediction from incomplete observations. In *CVPR*, 2021. [2](#)
- [7] Wenliang Dai, Junnan Li, Dongxu Li, Anthony Tiong, Junqi Zhao, Weisheng Wang, Boyang Li, Pascale N Fung, and Steven Hoi. Instructblip: Towards general-purpose vision-language models with instruction tuning. *Advances in neural information processing systems*, 36:49250–49267, 2023. [3](#)
- [8] Zhongbin Fang, Xiangtai Li, Xia Li, Joachim M Buhmann, Chen Change Loy, and Mengyuan Liu. Explore in-context learning for 3d point cloud understanding. *NeurIPS*, 2023. [2](#)
- [9] Dong Feng, Ping Guo, Encheng Peng, Mingmin Zhu, Wen-hao Yu, and Peng Wang. Posellava: Pose centric multimodal llm for fine-grained 3d pose manipulation. In *Proceedings of the AAAI Conference on Artificial Intelligence*, pages 2951–2959, 2025. [2, 5, 6](#)
- [10] Yao Feng, Jing Lin, Sai Kumar Dwivedi, Yu Sun, Priyanka Patel, and Michael J Black. Chatpose: Chatting about 3d human pose. In *Proceedings of the IEEE/CVF conference on computer vision and pattern recognition*, pages 2093–2103, 2024. [2, 3](#)
- [11] Félix G Harvey, Mike Yurick, Derek Nowrouzezahrai, and Christopher Pal. Robust motion in-betweening. *ACM TOG*, 2020. [2](#)
- [12] Alejandro Hernandez, Jurgen Gall, and Francesc Moren-Noguer. Human motion prediction via spatio-temporal inpainting. In *ICCV*, 2019. [2](#)
- [13] Catalin Ionescu, Dragos Papava, Vlad Olaru, and Cristian Sminchisescu. Human3. 6m: large scale datasets and predictive methods for 3d human sensing in natural environments. *IEEE T-PAMI*, 2013. [2, 5, 6, 7](#)
- [14] Biao Jiang, Xin Chen, Wen Liu, Jingyi Yu, Gang Yu, and Tao Chen. Motiongpt: Human motion as a foreign language. *Advances in Neural Information Processing Systems*, 36:20067–20079, 2023. [2, 3, 4, 5, 6, 9](#)
- [15] Manuel Kaufmann, Emre Aksan, Jie Song, Fabrizio Pece, Remo Ziegler, and Otmar Hilliges. Convolutional autoencoders for human motion infilling. In *3DV*, 2020. [2](#)
- [16] Yiheng Li, Ruibing Hou, Hong Chang, Shiguang Shan, and Xilin Chen. Unipose: A unified multimodal framework for human pose comprehension, generation and editing. In *Proceedings of the Computer Vision and Pattern Recognition Conference*, pages 27805–27815, 2025. [2, 3, 5, 6](#)
- [17] Haotian Liu, Chunyuan Li, Qingyang Wu, and Yong Jae Lee. Visual instruction tuning. *Advances in neural information processing systems*, 36:34892–34916, 2023. [3](#)
- [18] Mengyuan Liu and Junsong Yuan. Recognizing human actions as the evolution of pose estimation maps. In *CVPR*, 2018. [1, 2](#)
- [19] Mengyuan Liu, Xinshun Wang, Zhongbin Fang, Deheng Ye, Xia Li, Tao Tang, Songtao Wu, Xiangtai Li, and Ming-Hsuan Yang. Human-in-context: Unified cross-domain 3d human motion modeling via in-context learning. *arXiv preprint arXiv:2508.10897*, 2025. [2, 5, 6, 7, 8, 3](#)
- [20] Julieta Martinez, Rayat Hossain, Javier Romero, and J. Little. A simple yet effective baseline for 3d human pose estimation. *2017 IEEE International Conference on Computer Vision (ICCV)*, pages 2659–2668, 2017. [3](#)
- [21] Dario Pavllo, Christoph Feichtenhofer, David Grangier, and Michael Auli. 3d human pose estimation in video with temporal convolutions and semi-supervised training. *2019 IEEE/CVF Conference on Computer Vision and Pattern Recognition (CVPR)*, pages 7745–7754, 2018. [3](#)
- [22] Arkaprava Sinha, Dominick Reilly, Francois Bremond, Pu Wang, and Srijan Das. Ski models: Skeleton induced vision-language embeddings for understanding activities of daily

living. In *Proceedings of the AAAI Conference on Artificial Intelligence*, pages 6931–6939, 2025. 2

[23] Ke Sun, Bin Xiao, Dong Liu, and Jingdong Wang. Deep high-resolution representation learning for human pose estimation. In *Proceedings of the IEEE/CVF conference on computer vision and pattern recognition*, pages 5693–5703, 2019. 4, 6

[24] Xiao Sun, Bin Xiao, Shuang Liang, and Yichen Wei. Integral human pose regression. In *European Conference on Computer Vision*, 2017. 3

[25] Alexander Toshev and Christian Szegedy. Deeppose: Human pose estimation via deep neural networks. *2014 IEEE Conference on Computer Vision and Pattern Recognition*, pages 1653–1660, 2013. 3

[26] Aaron Van Den Oord, Oriol Vinyals, et al. Neural discrete representation learning. *Advances in neural information processing systems*, 30, 2017. 2

[27] Timo Von Marcard, Roberto Henschel, Michael J Black, Bodo Rosenhahn, and Gerard Pons-Moll. Recovering accurate 3d human pose in the wild using imus and a moving camera. In *ECCV*, 2018. 2, 6, 7

[28] Dongkai Wang, Shiyu Xuan, and Shiliang Zhang. Locllm: Exploiting generalizable human keypoint localization via large language model. In *Proceedings of the IEEE/CVF Conference on Computer Vision and Pattern Recognition (CVPR)*, 2024. 2, 5, 6, 3

[29] Xinshun Wang, Qiongjie Cui, Chen Chen, and Mengyuan Liu. Gcnext: towards the unity of graph convolutions for human motion prediction. In *AAAI*, 2024. 2

[30] Xinshun Wang, Zhongbin Fang, Xia Li, Xiangtai Li, Chen Chen, and Mengyuan Liu. Skeleton-in-context: unified skeleton sequence modeling with in-context learning. In *CVPR*, 2024. 2, 5, 6, 8

[31] Xinshun Wang, Wanying Zhang, Can Wang, Yuan Gao, and Mengyuan Liu. Dynamic dense graph convolutional network for skeleton-based human motion prediction. *IEEE T-IP*, 2024. 2

[32] Qinghao Ye, Haiyang Xu, Guohai Xu, Jiabo Ye, Ming Yan, Yiyang Zhou, Junyang Wang, Anwen Hu, Pengcheng Shi, Yaya Shi, et al. mplug-owl: Modularization empowers large language models with multimodality. *arXiv preprint arXiv:2304.14178*, 2023. 3

[33] Dewen Zhang, Tahir Hussain, Wangpeng An, and Hayaru Shouno. Llava-pose: Enhancing human pose and action understanding via keypoint-integrated instruction tuning. *arXiv preprint arXiv:2506.21317*, 2025. 2, 3

[34] Feng Zhang, Xiatian Zhu, Hanbin Dai, Mao Ye, and Ce Zhu. Distribution-aware coordinate representation for human pose estimation. In *CVPR*, 2020. 1, 2

[35] Xinyi Zhang, Qiqi Bao, Qinpeng Cui, Wenming Yang, and Qingmin Liao. Pose magic: efficient and temporally consistent human pose estimation with a hybrid mamba-gcn network. *arXiv preprint arXiv:2408.02922*, 2024. 1, 2, 3

[36] Ce Zheng, Sijie Zhu, Mat'ias Mendieta, Taojiannan Yang, Chen Chen, and Zhengming Ding. 3d human pose estimation with spatial and temporal transformers. *2021 IEEE/CVF International Conference on Computer Vision (ICCV)*, pages 11636–11645, 2021. 3

[37] Yi Zhou, Jingwan Lu, Connelly Barnes, Jimei Yang, Sitao Xiang, et al. Generative tweening: long-term inbetweening of 3d human motions. *arXiv preprint arXiv:2005.08891*, 2020. 2

[38] Bingfan Zhu, Biao Jiang, Sunyi Wang, Shixiang Tang, Tao Chen, Linjie Luo, Youyi Zheng, and Xin Chen. Motionpt3: Human motion as a second modality. *arXiv preprint arXiv:2506.24086*, 2025. 2, 5, 6

[39] Wentao Zhu, Xiaoxuan Ma, Zhaoyang Liu, Libin Liu, Wayne Wu, and Yizhou Wang. Motionbert: a unified perspective on learning human motion representations. In *ICCV*, 2023. 2, 5, 6, 7

[40] Xizhou Zhu, Weijie Su, Lewei Lu, Bin Li, Xiaogang Wang, and Jifeng Dai. Deformable detr: Deformable transformers for end-to-end object detection. *arXiv preprint arXiv:2010.04159*, 2020. 5

Superman: Unifying Skeleton and Vision for Human Motion Perception and Generation

Supplementary Material

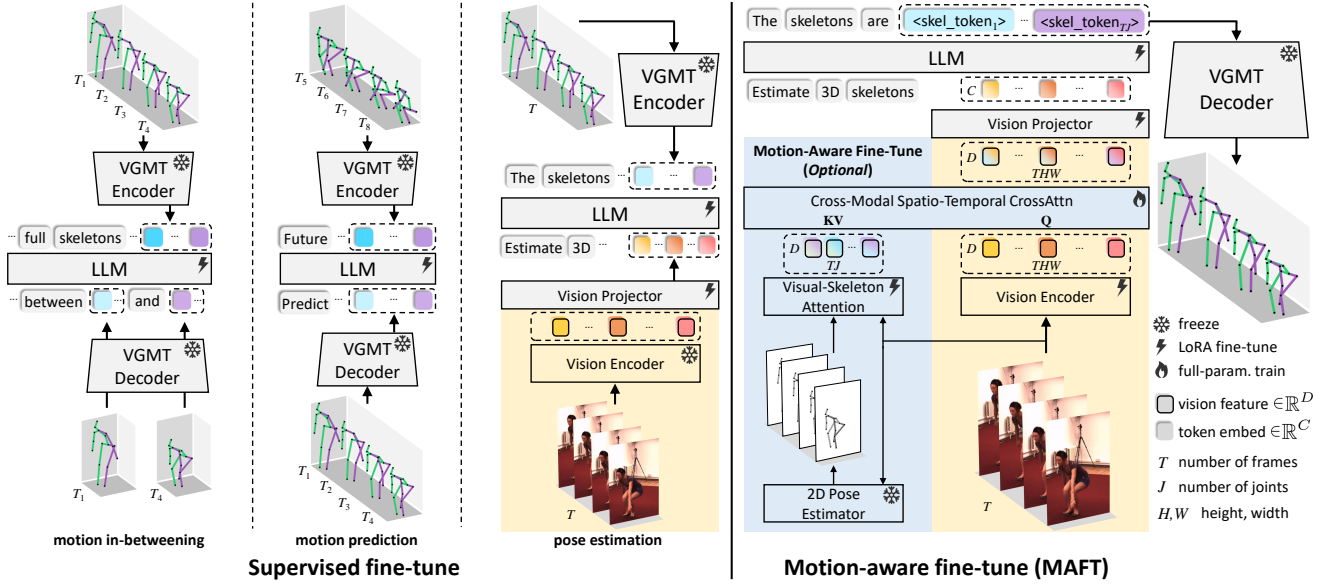


Figure S1. **Detailed Data Flow and Training Pipelines for Different Tasks.** **Left:** For generation tasks like *Motion In-betweening* and *Motion Prediction*, the model operates in a "Skeleton-to-Skeleton" mode. Historical or keyframe skeletons are tokenized by the frozen VGMT Encoder, and the LLM autoregressively predicts the missing/future tokens. **Right:** For *Pose Estimation*, the model operates in a "Video-to-Skeleton" mode. We compare the standard Supervised Fine-Tuning (SFT) pipeline against our proposed **Motion-Aware Fine-Tuning (MAFT)**. The MAFT pipeline explicitly injects skeletal geometry into the visual stream via the VSA module, enhancing feature alignment before LLM processing.

A. Implementation Details

A.1. Training Strategy

Tokenizer Training: The VGMT is trained for 500000 steps on Human3.6M. We use the AdamW optimizer with a learning rate of 0.0002 and batch size 256.

Unified MLLM Tuning: As shown in Fig. S1, unified MLLM tuning includes: 1) *Multi-Task Instruction Tuning*. We adopt a joint training strategy where data from all three tasks—3D Pose Estimation, Motion Prediction, and Motion In-betweening—are mixed within each batch. To unify these disparate tasks, we utilize the specific instruction templates to convert raw multi-modal data into a standardized "User-Assistant" conversation format. The model is optimized using a standard autoregressive cross-entropy loss over output tokens. 2) *Optional MAFT Integration*. For tasks involving video input (i.e., 3D Pose Estimation), we incorporate the Motion-Aware Fine-Tuning (MAFT) module. This light-weight component (adding < 0.2% trainable parameters) injects skeletal geometric priors into the visual stream via the Visual-Skeleton Attention (VSA) mech-

anism, enabling the MLLM to better attend to motion-relevant visual features. 3) *Hyper-parameters*. The MLLM is fine-tuned for 3 epochs. We use a learning rate of $1e-4$ with a cosine decay scheduler and a warmup ratio of 0.1. The global batch size is set to 16. All experiments are conducted on 2 NVIDIA H20 GPUs using PyTorch.

A.2. Instruction Templates

To unify diverse motion analysis tasks within a single MLLM framework, we employ instruction tuning. We convert raw data (videos and skeleton sequences) into a standardized conversation format, where the user provides an instruction containing multimodal inputs (e.g., `<video>`, `<skeleton>`), and the model generates the corresponding target skeleton tokens. Tab. S1 details the specific instruction templates used for each task during the training.

- **Vid2Skel (3D Pose Estimation):** The model inputs visual tokens (and optional 2D estimated poses) and is instructed to describe the motion using skeleton tokens.
- **SkelPred (Motion Prediction):** The model inputs a history sequence of skeleton tokens and predicts future frames. Both sequences contain 16 frames (320ms).

Table S1. **Instruction Templates for Multi-Task Training.** We utilize specific text prompts to guide the MLLM for different tasks. The bottom section illustrates a concrete example of the actual input prompt (with special vision tokens) and the corresponding output response.

Task	Input Modality	Instruction Template (User Prompt)	Output
3D Pose Estimation (Vid2Skel)	Video	Please describe the motion of the person in the video <video> using skeleton tokens. Your response should be formatted as: "Frame 1: torso: ... left_arm: ... right_arm: ... left_leg: ... right_leg: ... Frame 2: ..."	Skeleton Tokens ($K_{1:T}$)
Motion Prediction (SkelPred)	History Skeleton	Here's a motion sequence represented using skeleton tokens: <skeleton> Predict the future motion using skeleton tokens that have the same number of frames as the history motion. Your response should be formatted as: "Future Frame 1: torso: ... left_arm: ... right_arm: ... left_leg: ... right_leg: ... Future Frame 2: ..."	Future Skeleton Tokens
Motion In-betweening (MIB)	Start/End Keyframes	Here's a motion sequence with missing in-between frames. It contains only the start and end keyframes, represented using skeleton tokens: <skeleton> Generate the in-between frames to create a smooth transition between the provided keyframes. Your response should be formatted as a complete sequence: "Frame 1: ... left_arm: ... right_arm: ... left_leg: ... right_leg: ... Frame 2: ..."	Intermediate Skeleton Tokens

Real Input Prompt Example (with Special Tokens):

User: Please describe the motion of the person in the video <|vision_start|><|video_pad|>...<|video_pad|><|vision_end|> using skeleton tokens. Your response should be formatted as: "Frame 1: torso: ... left_arm: ... right_arm: ... left_leg: ... right_leg: ... Frame 2: ..."

Real Output Example (Body-Part Level Grouping):

Assistant: There are 4 frames in total. Here are the skeleton tokens for 5 body parts in each frame:

Frame 1: torso: <skel_1848><skel_7294><skel_188><skel_5434><skel_975>. left_arm: <skel_5563><skel_6334><skel_7382>. right_arm: <skel_1656><skel_7242><skel_7368>. left_leg: <skel_4964><skel_445><skel_426>. right_leg: <skel_2974><skel_3963><skel_1134>. Frame 2: torso: <skel_7234><skel_7612><skel_7832><skel_2617><skel_3466>. left_arm: <skel_2904><skel_165><skel_5270>. ...

- **MotionInBetween (In-betweening):** The model inputs sparse keyframes (start and end) and generates the intermediate transition sequence.

B. Additional Visualization Results

We further demonstrate the superiority of *Superman* through qualitative comparisons across tasks.

B.1. Robustness in 3D Pose Estimation

Fig. S2 presents a visual comparison for pose estimation.

- **Correction of Upstream Errors:** The bottom block of Fig. S2 highlights a challenging scenario where the off-the-shelf 2D pose estimator (CPN [5]) fails to detect the right foot due to motion blur (see red box). Baseline methods like HiC [19], which rely heavily on 2D key-points, propagate this error into the final 3D output.
- **Effect of MAFT:** Our model with Motion-Aware Fine-Tuning (MAFT) effectively mitigates this issue. By lever-

aging the Cross-Attention mechanism to query visual features directly from the video, *Superman* “looks back” at the raw frames to recover the missing foot information.

B.2. Temporal Coherence in Motion Prediction

Fig. S3 compares the prediction capabilities on the Human3.6M dataset. The task involves predicting 320ms of future motion based on historical context. As observed in the “Sitting” sequence, baseline methods such as MotionGPT3 [38] and HiC [19] tend to generate stiff or slightly drifting motions as time progresses. In contrast, *Superman* maintains high temporal fidelity, accurately predicting the descent of the body and the knee bending trajectory, closely matching the ground truth.

B.3. Generalization in Motion In-betweening

Fig. S4 evaluates the Motion In-betweening task, where the model must synthesize a coherent sequence connecting a

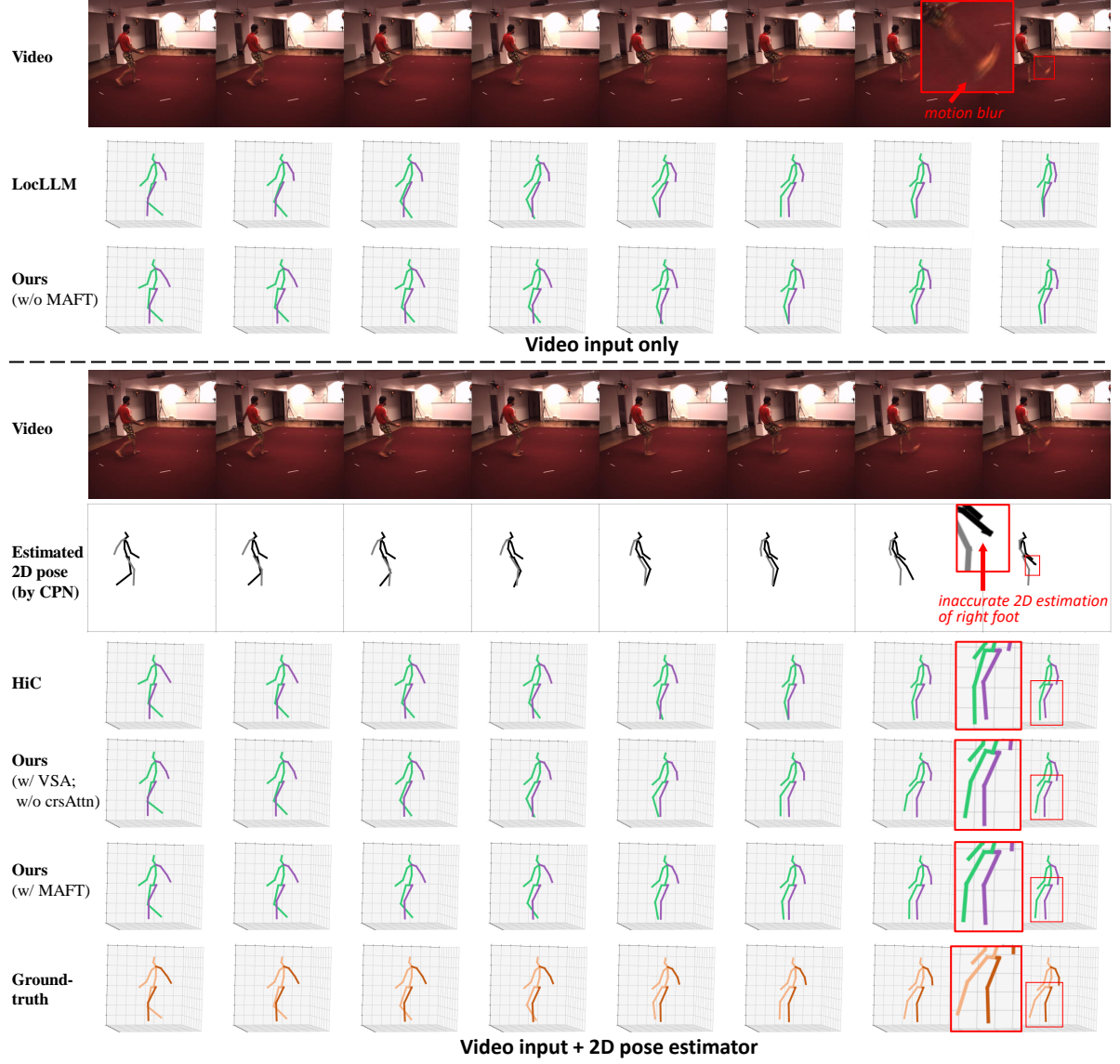


Figure S2. **Qualitative Results for 3D Pose Estimation on Human3.6M: The Impact of MAFT.** **Top Block (Video Input Only):** Compared to LocLLM [28], our method (even without MAFT) generates more physically plausible poses from raw video, handling motion blur more effectively. **Bottom Block (Video + 2D Pose Input):** This case highlights the robustness of our MAFT module. The off-the-shelf 2D pose estimator (CPN [5]) fails to detect the right foot due to occlusion/blur (see red box). Consequently, the baseline HiC [19], which relies heavily on 2D inputs, produces an erroneous pose. In contrast, **Ours (w/ MAFT)** successfully corrects this error by attending to the visual features via the cross-attention mechanism, recovering the correct leg position that matches the Ground Truth.

start and an end frame.

- **In-Domain (Human3.6M):** In the top row, our model generates a smooth turning motion, naturally interpolating the limb rotations.
- **Out-of-Domain (3DPW):** The bottom row demonstrates generalization on the unseen 3DPW dataset. Despite never being trained on this data, *Superman* synthesizes a realistic stepping motion. Comparison methods often struggle with such large gaps or unseen poses, resulting in artifacts. Our success here attributes to the robust, vision-

grounded motion vocabulary learned by the VGMT.

C. Visualization of Intermediate Features

In this chapter, we "open the black box" of *Superman* by visualizing the intermediate representations learned by its key components. This provides qualitative evidence for the mechanisms of VSA sampling, MAFT attention, and the semantic structure of the learned codebook.

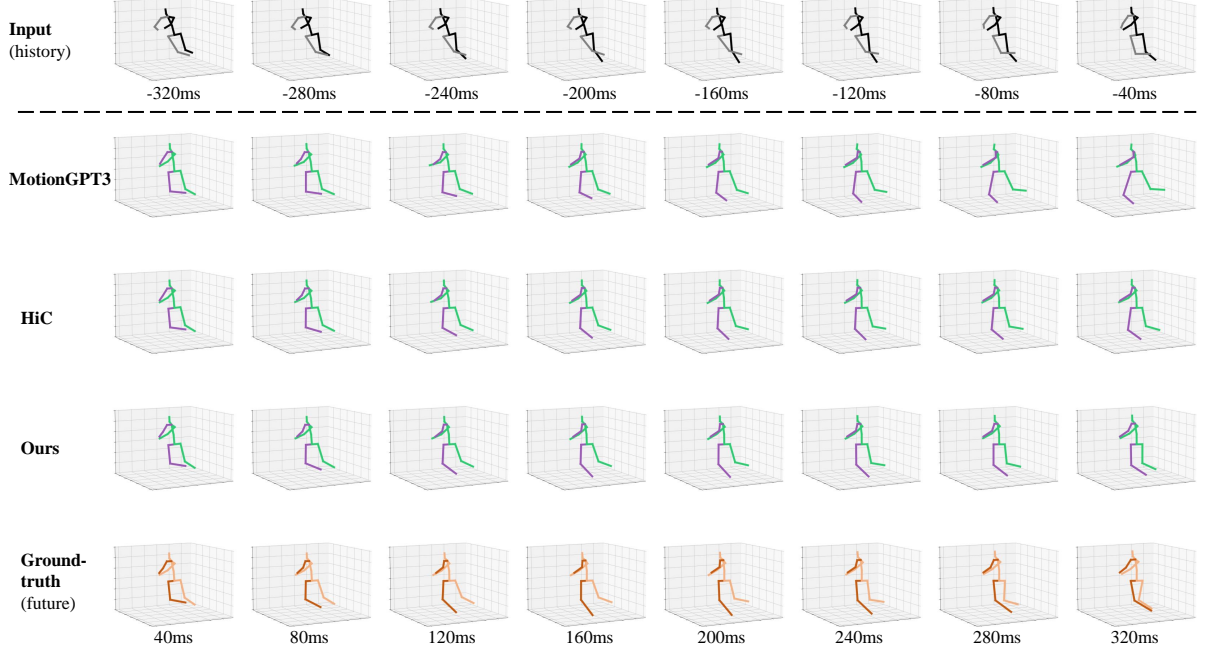


Figure S3. **Qualitative Comparison for Motion Prediction on Human3.6M.** The model predicts the future 320ms motion given a history sequence (grey). While baselines like MotionGPT3 [36] and HiC [17] exhibit slight temporal jitter or drift in the leg positioning during the "Sitting" action, **Superman (Ours)** generates a smooth and accurate trajectory that closely aligns with the Ground Truth (orange), demonstrating superior temporal coherence.

C.1. Adaptive Sampling in VSA

A critical challenge in vision-guided motion generation is the unreliability of upstream 2D pose estimators, particularly under rapid motion or occlusion. To validate how our Visual-Skeleton Attention (VSA) module addresses this, we visualize the internal sampling process in Fig. S5 & S6.

Visualization Protocol: We visualize the sampling behavior of different attention heads across temporal frames. In the visualization:

- The **Start Point** of a green line represents the initial reference point provided by the off-the-shelf 2D pose estimator (CPN).
- The **Green Line** represents the learned offset vector (Δp) predicted by the VSA module.
- The **End Point (Green Circle)** indicates the final adaptive sampling location on the feature map.
- The **Area of the Circle** corresponds to the learned attention weight, where larger circles indicate higher contribution to the aggregated feature.

Analysis of Correction Capability: As highlighted in the bottom row of Fig. S5 (Frame 8), the fast-moving right foot causes significant motion blur, leading the fixed 2D estimator to incorrectly localize the joint on the leg or background (see the white dot). However, our VSA module detects this semantic misalignment. The predicted offsets (green lines) diverge from the erroneous initial point and accurately point towards the actual "ghosting" region of the

blurry foot. Furthermore, different attention heads (Head 1-4) learn to focus on complementary features—some attending to the heel and others to the toe trajectory—aggregating a robust visual representation despite the noisy input. This confirms that VSA functions not just as a sampler, but as a dynamic *visual corrector*.

Fig. S6 demonstrates the tracking of the left foot. Even when the 2D estimation is relatively stable, the VSA module actively refines the sampling points. Different attention heads (Head 1-4) can be seen focusing on distinct semantic parts (e.g., heel vs. toe) or expanding the receptive field to capture context, ensuring a rich feature representation.

C.2. Cross-Modal Spatio-Temporal Attention in MAFT

We analyze the cross-attention maps in MAFT from two perspectives: (1) Cross-Frame Temporal Tracking and (2) Cross-Joint Semantic Alignment.

C.2.1. Spatio-Temporal Consistency (Cross-Frame)

We visualize how specific skeletal queries attend to visual features across frames.

- **Right Elbow (Fig. S9) & Right Shoulder (Fig. S10):** In this bending motion, the attention hotspot tracks the downward movement of the upper body joints.
- **Right Ankle (Fig. S7) & Right Wrist (Fig. S8):** In this dynamic kicking sequence, the attention precisely follows the limb trajectory. Notably, for the Right Ankle, the

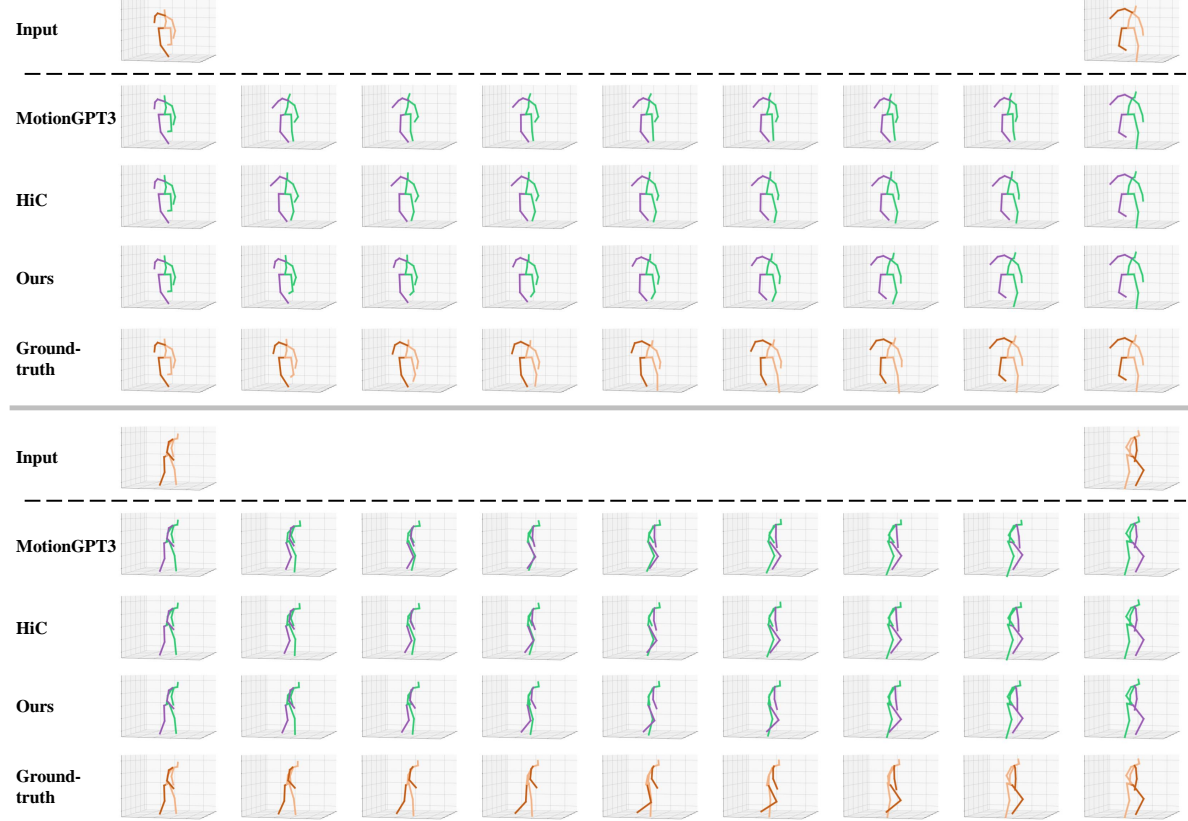


Figure S4. **Qualitative Results for Motion In-betweening on Human3.6M and 3DPW.** The task is to generate the intermediate motion sequence given only the first and last frames (Input). **Top Row (Human3.6M):** Our model generates a natural transition for the turning action, whereas MotionGPT3 struggles with the limb orientation. **Bottom Row (3DPW):** On the unseen 3DPW dataset, our model demonstrates strong generalization, synthesizing a realistic stepping motion that bridges the gap smoothly, outperforming comparison methods.

hotspot shifts from the floor (Frame 2) to mid-air (Frame 8), confirming robust temporal tracking.

C.2.2. Fine-Grained Semantic Alignment (Cross-Joint)

To confirm semantic disentanglement, we visualize attention maps for *different joint queries* within the same frames. As shown in Figures S11 and S12, changing the query token shifts the attention focus dramatically (e.g., from "R_Hip" torso region to "L_Ankle" feet region). This proves that MAFT establishes precise, part-level correspondence between modalities.

C.3. Semantic Analysis of the Codebook

Finally, to validate that our discrete tokens carry explicit physical meanings, we perform a "Semantic Sphere" analysis. For every code index k in the learned vocabulary, we calculate the average displacement vector of all motion segments assigned to it. We then visualize these vectors as fiber-like lines radiating from the origin, normalized to unit length to emphasize directionality.

Fig. S13 presents the results for four critical end-

effectors: **Left/Right Wrists** and **Left/Right Ankles**. These joints typically exhibit the highest degrees of freedom and complexity in human motion. Key observations:

- **Isotropic Coverage (No Mode Collapse):** As illustrated in the figure, the motion vectors for all four joints form dense, almost perfect spheres. The uniform distribution of vectors in every direction (isotropic) provides compelling evidence that our codebook effectively covers the full manifold of possible motion directions. There are no significant "holes" or gaps, indicating that the model has avoided mode collapse and can generate diverse motions in any 3D direction.
- **High-Fidelity Granularity:** The sheer density of the fibers—representing over 2,000 active codes for these end-effectors—confirms that the tokenizer captures fine-grained kinematic details. The model allocates a vast vocabulary to describe subtle variations in hand and foot movements, which is crucial for high-quality motion generation.
- **Directional Semantics:** The smooth transition of colors (representing azimuthal direction) confirms that the codes

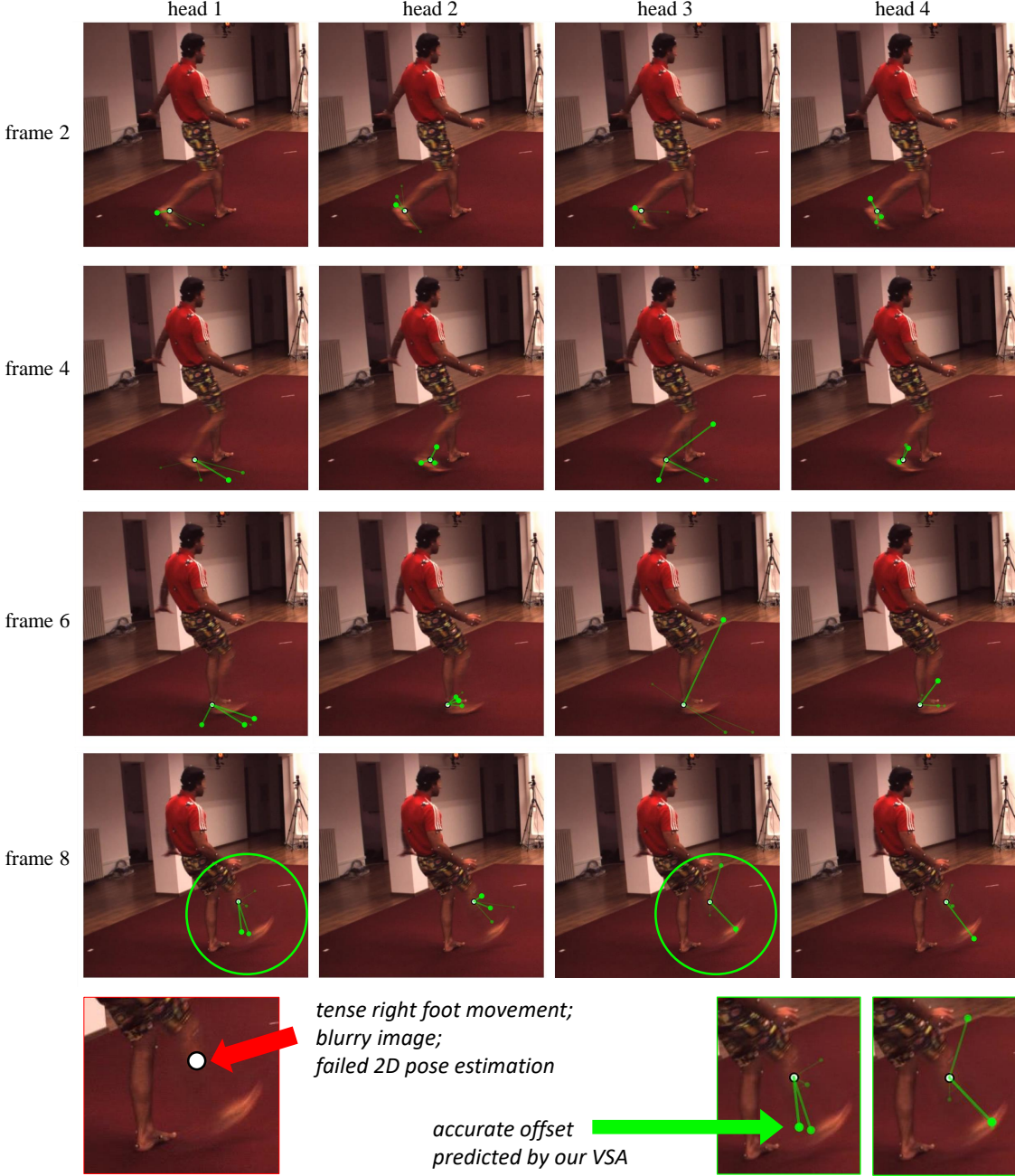


Figure S5. **Visualization of Adaptive Sampling in Visual-Skeleton Attention (VSA) – Right foot as an example.** We visualize the learned sampling offsets and weights for different attention heads (columns) across video frames (rows). The **start point** of each green line indicates the initial, potentially noisy 2D keypoint estimated by CPN. The **green line** represents the predicted offset, pointing to the **green circle** which denotes the final sampling location. The **area** of the green circle reflects the attention weight assigned to that sampling point. **Highlight (Bottom Row):** In Frame 8, rapid motion causes the right foot to blur, leading to a failed 2D estimation (white dot). Our VSA module successfully identifies the error, predicting large offsets that redirect attention from the erroneous leg position back to the true, blurry foot region (red and green boxes), thereby ensuring robust feature extraction.

are semantically organized. Specific codes map uniquely to specific physical directions, allowing the subsequent MLLM to control motion with precise directional intent.

C.4. Feature Analysis: Before vs. After MAFT

To visually validate the impact of the Motion-Aware Fine-Tuning (MAFT) module on visual feature representation,

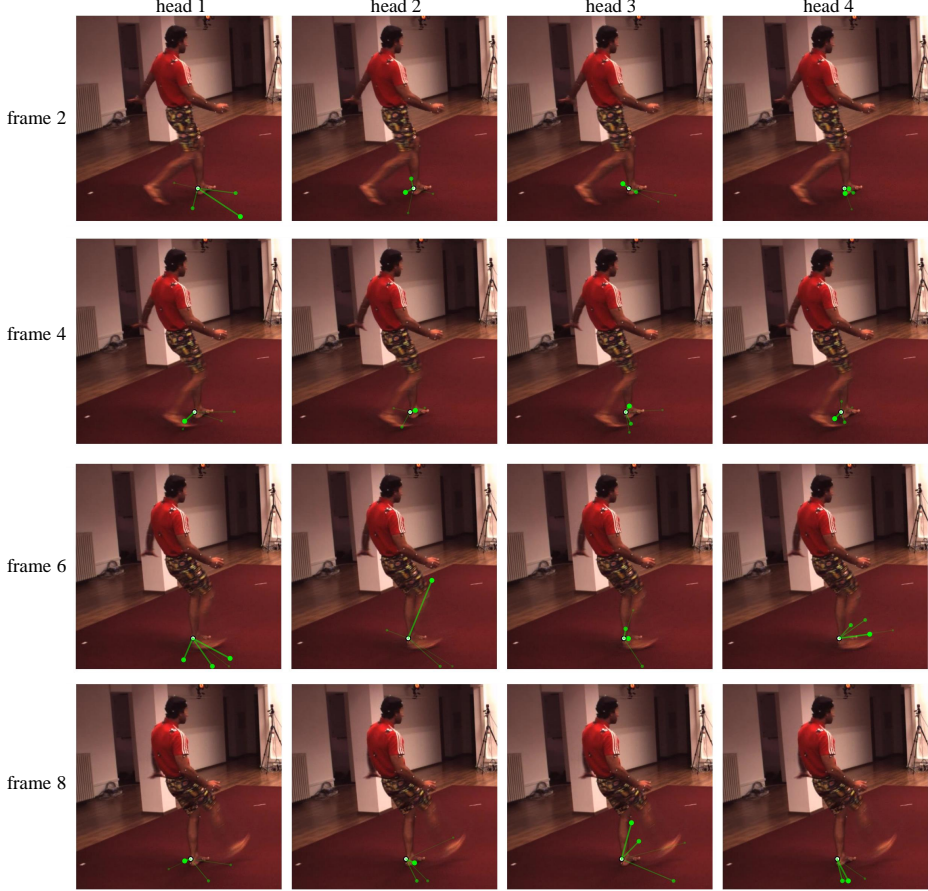


Figure S6. **Visualization of Adaptive Sampling in Visual-Skeleton Attention (VSA) – Left foot as an example.** The VSA sampling process for the planting and lifting phase of the left foot is illustrated. **Multi-Head Diversity:** Different attention heads exhibit diverse sampling strategies. For instance, while Head 2 tends to focus tightly on the joint center (small offsets), Head 4 explores a wider neighborhood (larger offsets) to capture contextual motion cues. This diversity allows the model to build a robust representation of the limb’s state even during complex articulation.

we compare the attention activation maps *before* and *after* the Cross-Attention fusion layer. The results for four distinct motion samples are presented in Figures S14 and S15.

- **Before MAFT (Pre-Fusion):** The attention maps (middle columns) exhibit scattered, noisy activations. The model attends to various background elements or irrelevant body parts without a clear focus, indicating that the raw visual features lack specific geometric guidance.
- **After MAFT (Post-Fusion):** After processing by MAFT, the attention maps (right columns) become highly concentrated and structurally aligned with the human body. The heatmaps accurately highlight the entire human figure, effectively suppressing background noise.

This contrast confirms that MAFT successfully injects skeletal geometric priors into the visual stream, forcing the model to “focus” on the motion-relevant regions.

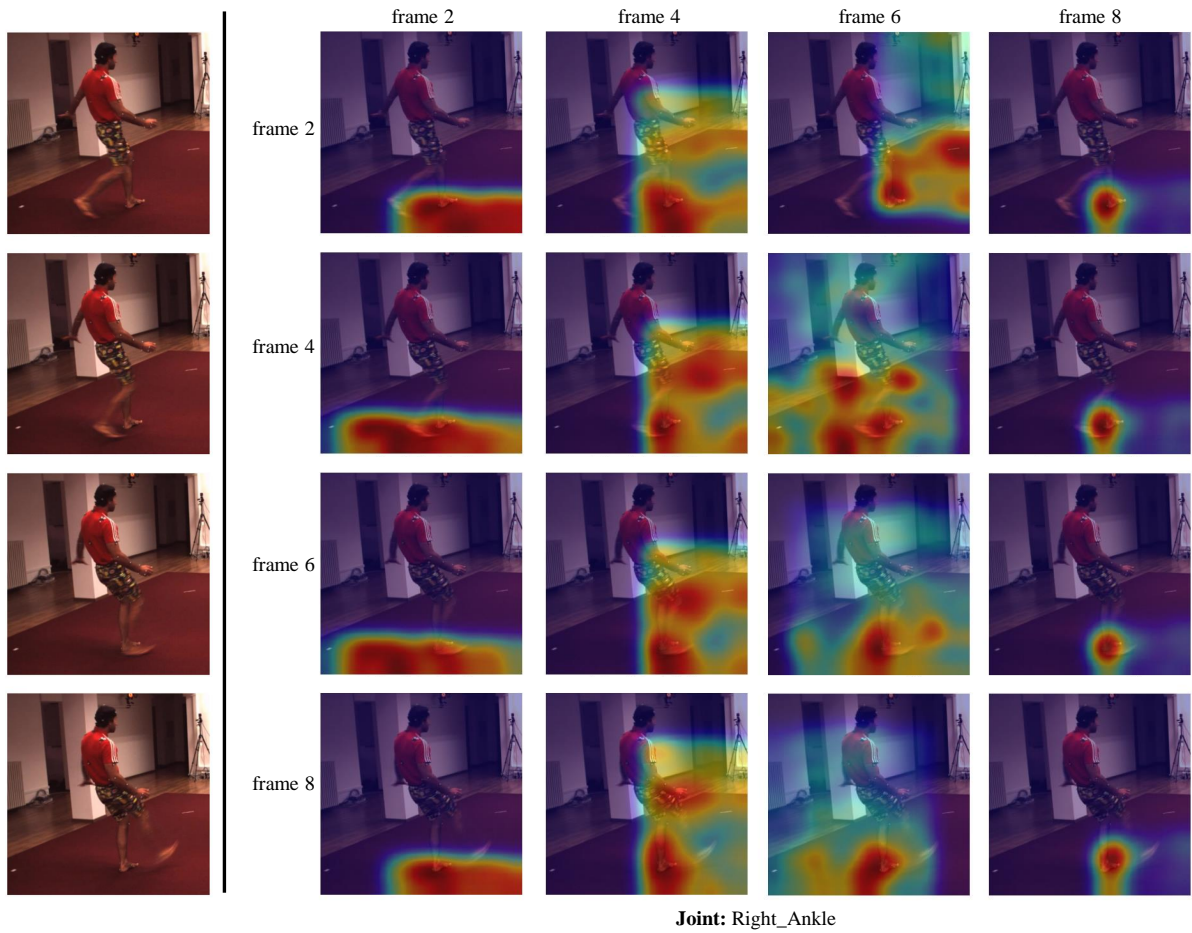


Figure S7. **Cross-Frame Attention: Right Ankle.** The attention hotspot (red) tracks the ankle lifting from the ground to mid-air.

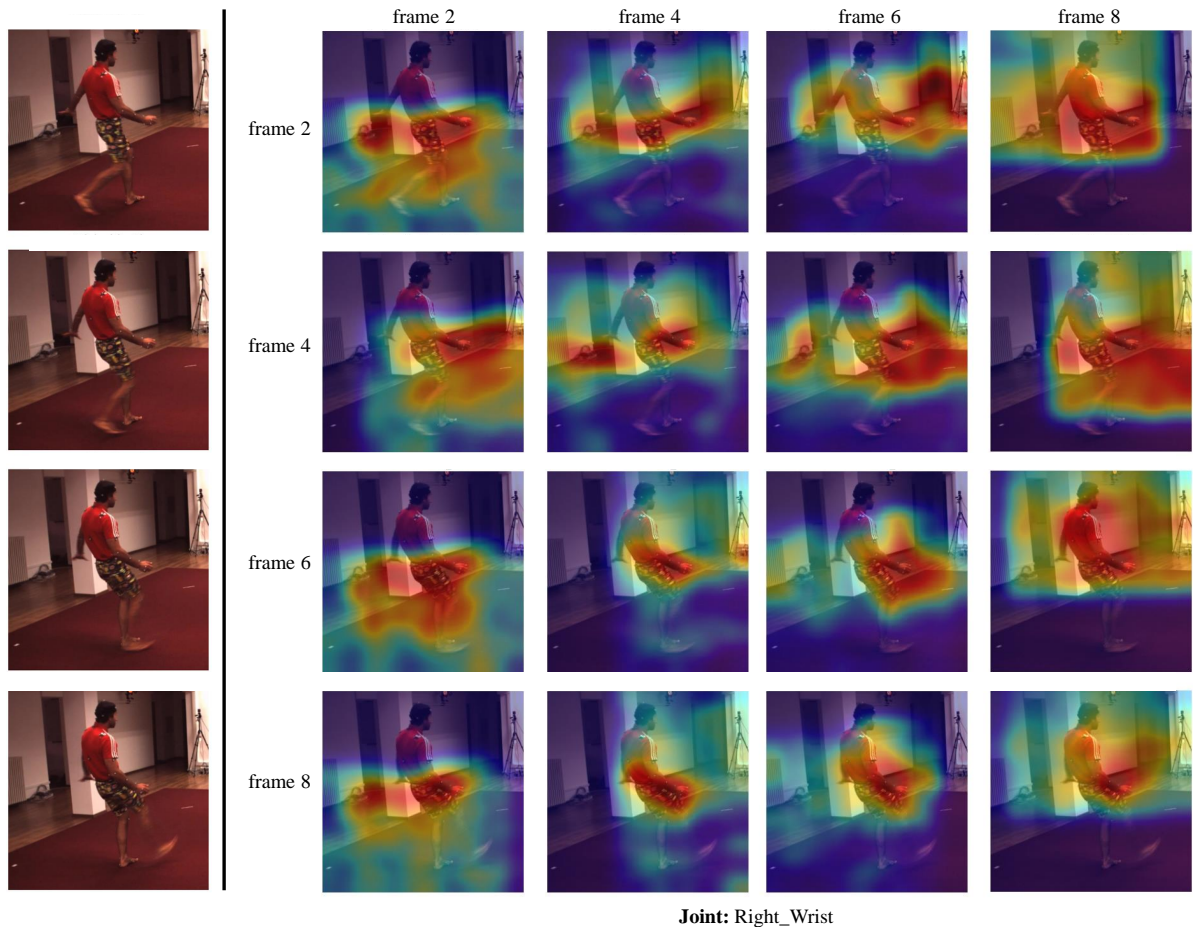


Figure S8. **Cross-Frame Attention: Right Wrist.** Attention follows the wrist during the arm swing.

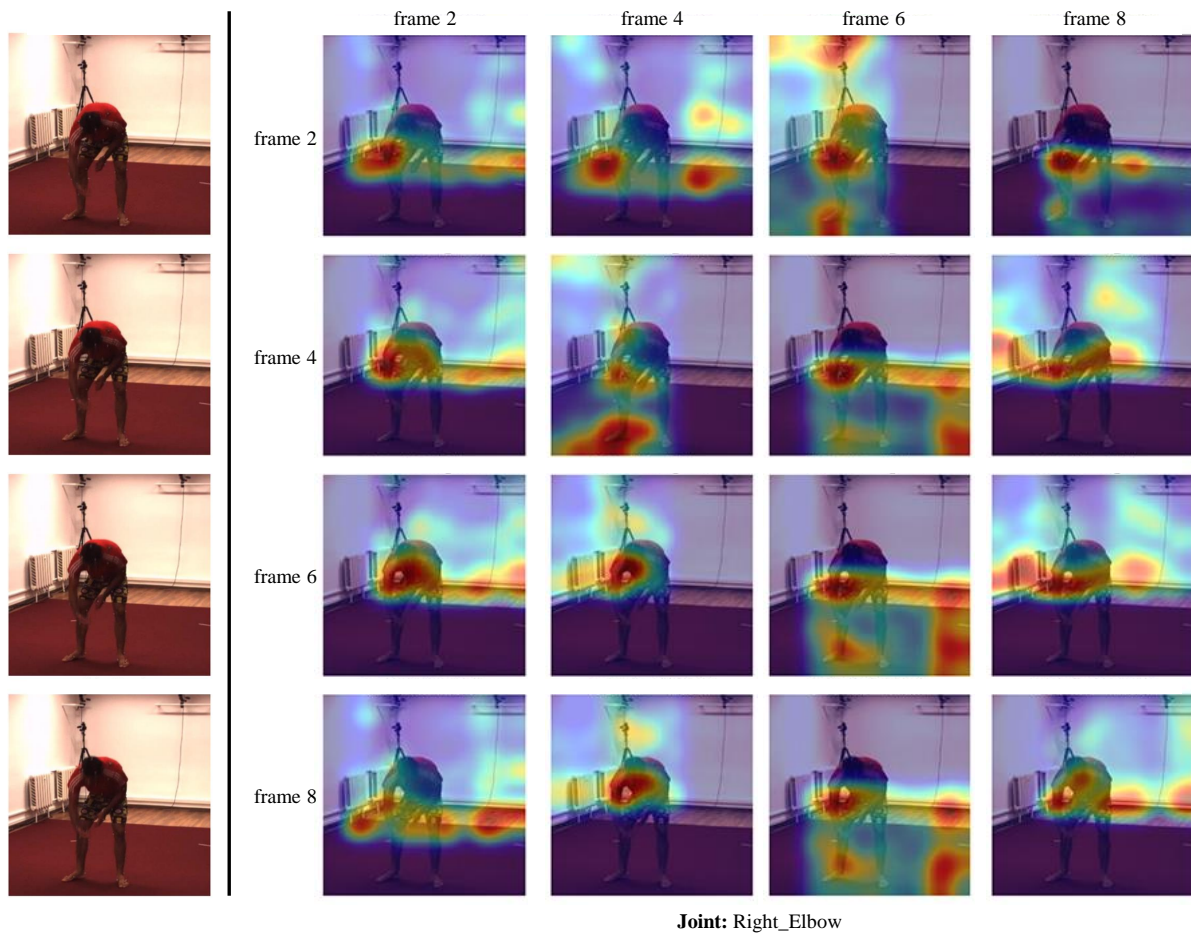


Figure S9. **Cross-Frame Attention: Right Elbow.** The model consistently tracks the elbow during a bending motion.

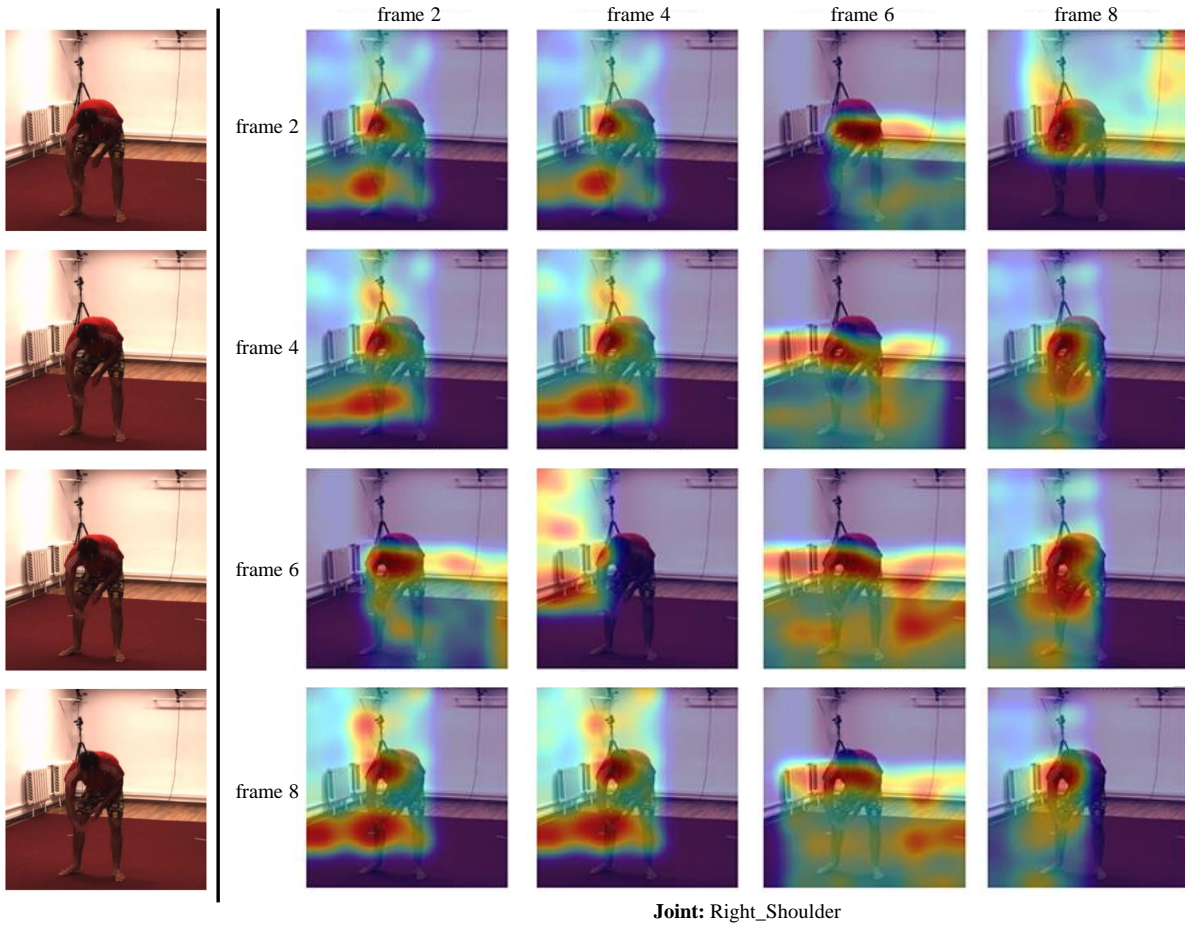


Figure S10. **Cross-Frame Attention: Right Shoulder.** Attention focuses on the shoulder region across frames.

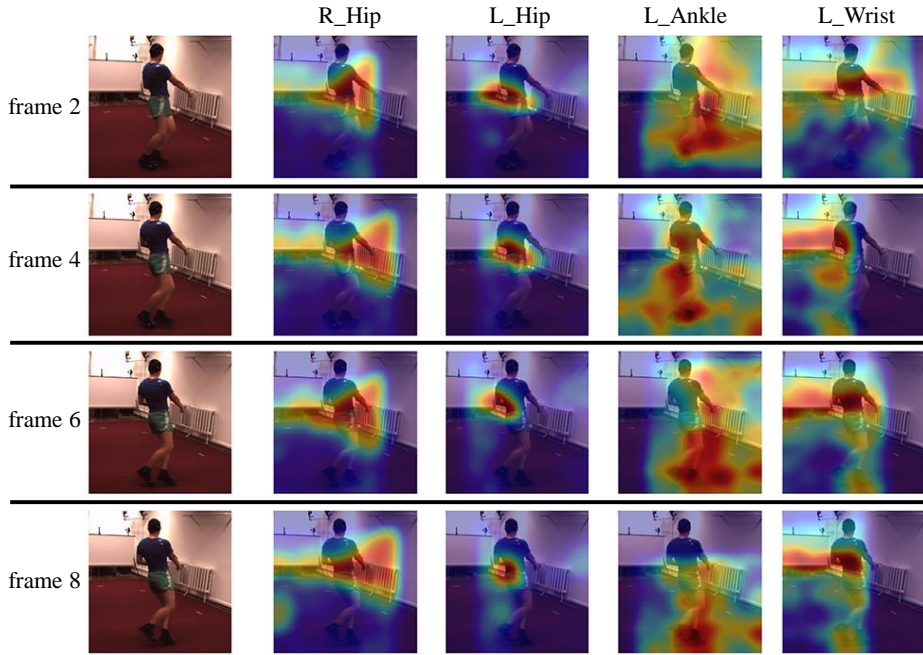


Figure S11. **Cross-Joint Semantic Alignment.** Distinct attention regions for Hip, Ankle, and Wrist queries.

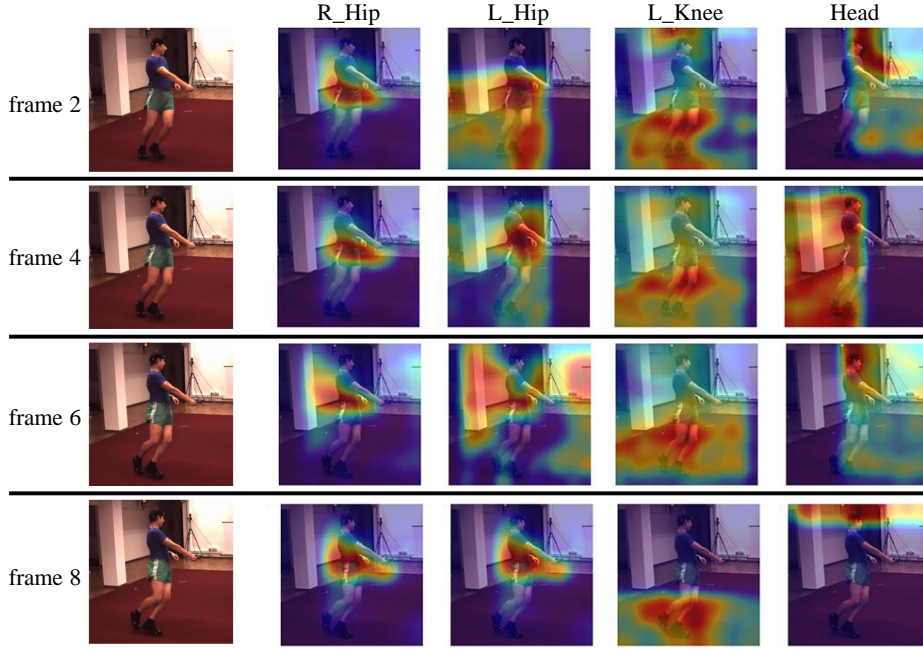


Figure S12. **Cross-Joint Semantic Alignment.** The model disentangles semantics, focusing on Head vs. Knee vs. Hip.

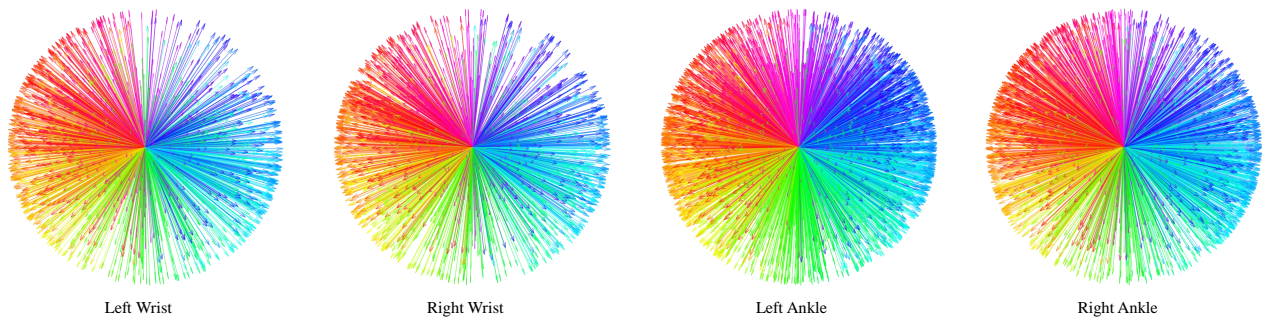


Figure S13. **Visualization of the “Semantic Spheres” of Motion Primitives across Different Joints.** Each sphere visualizes the discrete vocabulary learned by our Vision-Guided Motion Tokenizer (VGMT) for a specific body joint. Each fiber-like line represents a unique code in the codebook, plotted as its normalized average displacement vector (starting from the origin). The color indicates the motion direction (azimuthal hue). **(1) Omnidirectional Coverage:** The dense, isotropic spherical distribution demonstrates that the codebook effectively covers the full manifold of possible motion directions without mode collapse. **(2) High-Fidelity Granularity:** The high density of vectors (e.g., over 2,000 active codes for hands and feet) confirms that the tokenizer captures fine-grained kinematic details.

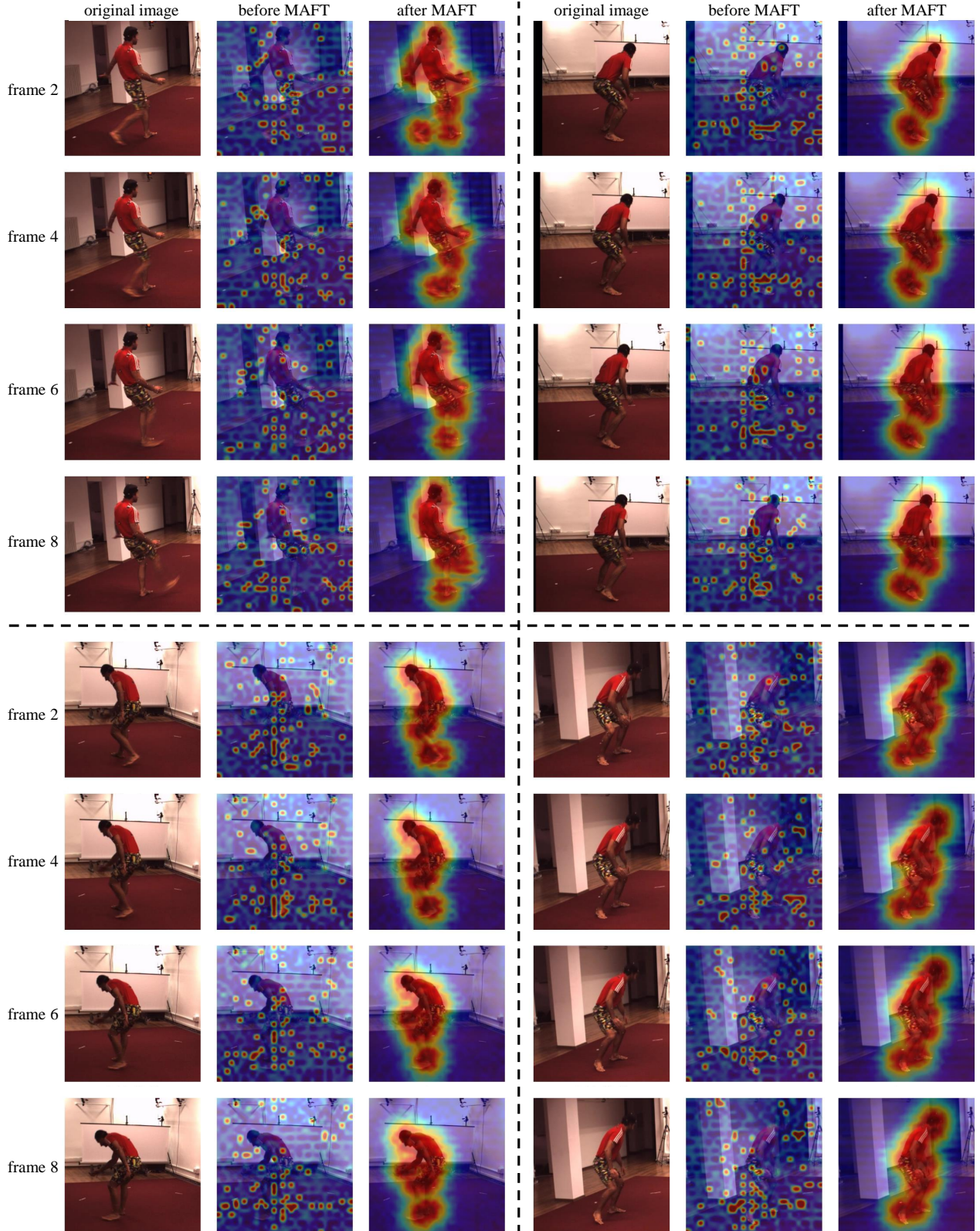


Figure S14. Visualization of Visual Features Before and After MAFT Fusion (Samples 1-4). We compare the attention maps of the visual features before entering the MAFT module (*middle column*) and after the Cross-Attention fusion (*right column*). **Before MAFT**, the features are scattered and noisy. **After MAFT**, the attention is significantly refined, focusing precisely on the human body and suppressing background clutter. This demonstrates that MAFT effectively aggregates semantic information guided by skeletal cues.

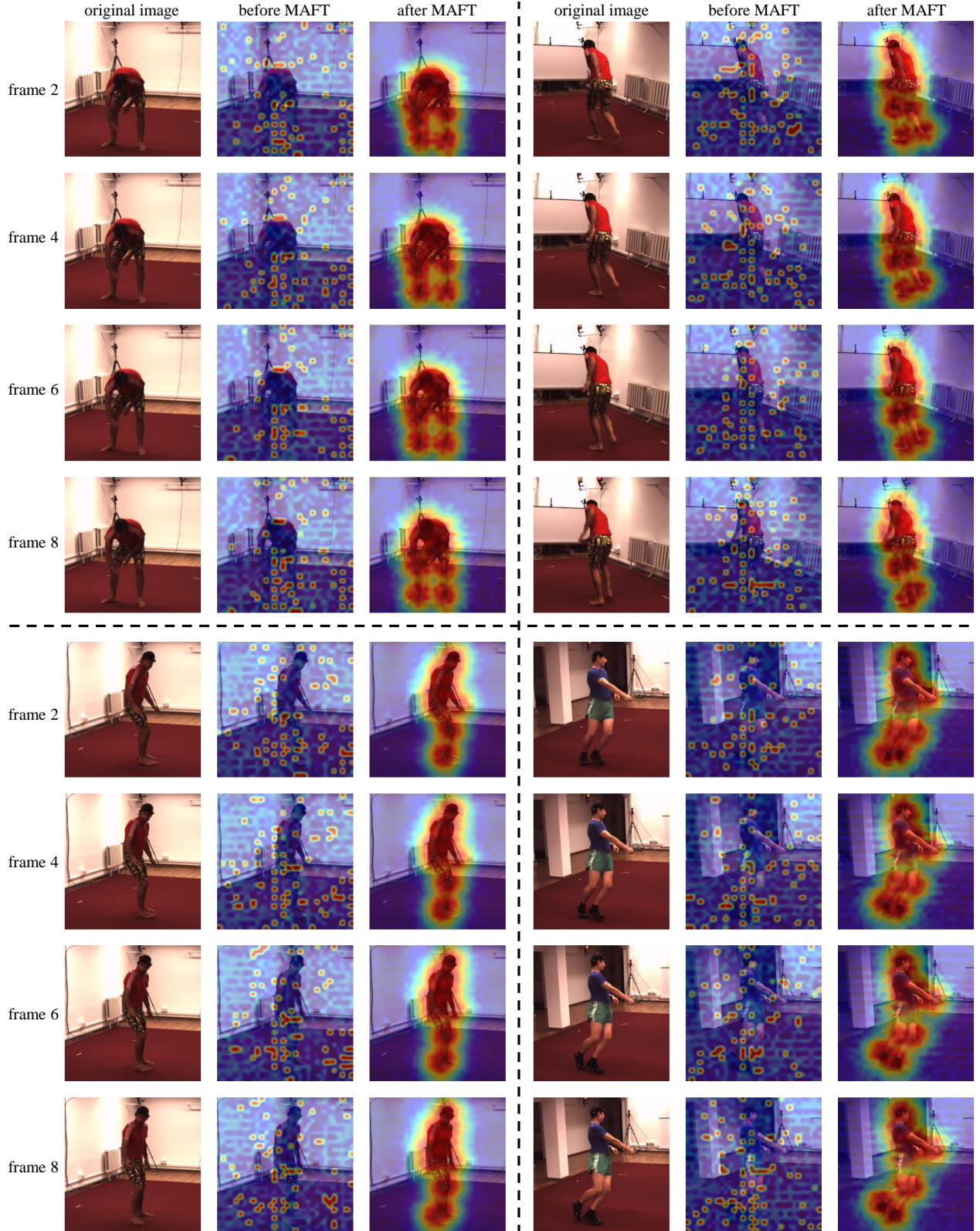


Figure S15. Visualization of Visual Features Before and After MAFT Fusion (Samples 5-8). Additional examples showing the focusing effect of MAFT. Regardless of the pose (bending, standing, or turning), the post-MAFT features (right) consistently show a strong, cohesive activation on the subject, proving the robustness of our geometric injection mechanism.